

https://dspace.org/

Gamma ray fluorescence for in situ evaluation of ore in Witwatersrand gold mines

Rolle, Rainer

2015-08-18
http://hdl.handle.net/10539/18258

Downloaded from a DSpace repository. https://dspace.org/

GAMMA RAY FLUORESCENCE FOR *IN SITU* EVALUATION OF ORE IN WITWATERSRAND GOLD MINES

R. ROLLE

GAMMA RAY FLUORESCENCE FOR *IN SITU* EVALUATION OF ORE IN WITWATERSRAND GOLD MINES

Rainer Rolle

A Thesis Submitted to the Faculty of Science
University of the Witwatersrand, Johannesburg
for the Degree of Doctor of Philosophy

Johannesburg 1979

ABSTRACT

A system for quantitative in situ evaluation of ore in Witwatersrand gold mines was researched and subsequently developed.

The principle of measurement is based on the excitation of gold K X-rays in rock face samples by the 88 keV gamma radiation from a Cadmium-109 radioisotope source. The X-rays and scattered radiation from the rock matrix are detected by a hyperpure germanium detector cooled by liquid nitrogen in a portable probe. In the fluorescence spectrum the intensity ratio of the gold $K\beta$ peaks to their immediate scattered background is evaluated and quantitatively converted in the portable analyser to area concentration units.

All aspects of the physical and instrumental measurement had to be investigated to arrive at a system capable of quantitative evaluation of trace concentrations in stope face ore samples. The parameters of efficiency of excitation of the gold K X-rays, and the energy distribution after scattering from the rock matrix at different angles were investigated from basic principles to determine an optimum source-sample-detector geometry which would allow quantitative evaluation of homogeneous ore concentrations. For edged-on measurement of rough-surfaced thin layer deposits a method of controlling the measurement geometry through ratemeter feedback was developed to allow conversion of mass concentration values to units of area concentration.

The parameters of spectrum evaluation were investigated from fundamental principles to allow qua titative assesement of different methods of peak evaluation for optimization of the method as a whole. The basic concepts of random signal processing times were developed together with new concepts of pileup parameters to allow a quantitative descriotion of the data acquisition rate of a complete analog pulse processing system.

With this foundation a practical measuring geometry and optimum values for signal processing time parameters, for detector size and for discriminator positions for spectrum evaluation could be determined.

Parallel with the derivation of optimum measurement parameters went the development of instruments, their field testing and appraisal of the method. The underground results obtained with prototype versions of the gamma ray fluorescence analyser were in all instances found to have a highly significant correlation with those obtained from the same locations by conventional chip or bulk sampling and fire assay.

The development of the gamma ray fluorescence method has shown the potential of the method to serve as an ore valuation tool and to assist in the geological identificaion of strata in Witwatersrand gold mines.

To NELMA

DECLARATION

The work presented in this thesis is my own and has not previously been submitted for a degree at any university.

R. Rolle

R. ROLLE

FEBRUARY 1979

ACKNOWLEDGEMENTS

This research was undertaken at the Metallurgy Laboratory of the Chamber of Mines Research Organisation, which is an extended campus of the University of the Witwatersrand, Johannesburg. The facilities made available by this laboratory are gratefully acknowledged.

The author wishes to express his sincere thanks to the following people:

Dr. P.J.D. Lloyd, the director of the Chamber of Mines Metallurgy Laboratory for the encouragement and understanding for this work through often difficult times.

Prof. J.P.F. Sellschop for his guidance, encouragement and understanding.

Prof. J.T. Moelwyn-Hughes for encouragement to continue the work.

Mr. T.A. Davies for his pleasant co-operation in looking after the instrumentation and the gathering of underground data.

Dr. P.J.D. Lloyd for permission to use the laboratory's HP9825 calculator for production of the manuscript.

Finally I wish to thank my wife Nelma, for her understanding and encouragement to complete this work, and for the final help in duplicating the manuscript.

CONTENTS

ABSTRACT ii

DEDICATION iv

DECLARATION v

ACKNOWLEDGEMENT vi

CONTENTS viii

LIST OF TABLES xi

LIST OF FIGURES xii

1 INTRODUCTION 1

1.1 Nature of the Witwatersrand gold deposits 1

1.2 Ore valuation 3

1.3 Alternative methods of evaluation of ores 8

1.4 Discussion 11

2 OUTLINE OF THE DEVELOPMENT OF THE FLUORESCENCE METHOD 14

2.1 Rock penetration for an instrumental method 14

2.2 Description of the fluorescence system 16

3 EXCITATION OF FLUORESCENT X-RAYS 20

3.1 Particle induced X-ray emission 21

3.2 Photon excitation 21

3.2.1 Bremsstrahlung sources 22

3.2.2 X-ray sources 22

3.2.3 Low energy gamma sources 23

3.3 Comparison of X-ray tubes and radioisotope sources 24

3.4 Radioisotope sources for excitation of gold K X-rays 24

3.4.1 Primary emission of potential radioisotopes 25

3.4.2 Secondary emissions from sources 25

3.4.3 The excitation spectrum in thick samples 27

3.4.4 Excitation of other heavy elements 31

4 THE BACKGROUND SPECTRUM 33

4.1 Photon scattering 34

4.2 Scattering spectrum from thick samples 38

4.3 Source - sample - detector geometry 40

5 DETECTION OF FLUORESCENT SPECTRA 46

5.1 Geometrical detection efficiency 46

5.1.1 Detector thickness 47

5.2 Energy resolution 48

5.2.1 Resolution of germanium detectors 50

6 FUNDAMENTALS IN SPECTRUM EVALUATION 54

6.1 Gaussian peak on a constant background 55

6.2 Generalized evaluation 56

6.3 Variance of the peak to background ratio 59

6.4 Comparison of multichannel and few channel methods 69

7 EVALUATION OF SPECTRA FOR GOLD ANALYSIS 73

7.1 Comparison of different peaks and backgrounds 73

7.2 Comparison of spectra from Cd-109, Co-57 and Te-123m 75

7.3 Measurement of the Cd-109 gold ore spectrum 79

8 FUNDAMENTALS IN SIGNAL PROCESSING 82

8.1 Extending and non-extending processing times 83

8.2 Processing overlap parameters 84

8.3 Effective processing times and efficiency 86

8.4 Relative importance of various processing parameters 88

8.5 Pileup rejection 90

8.6 Appendix: Derivation of equations 91

9 ANALOG SIGNAL PROCESSING IN THE GOLD ANALYSER 95

9.1 The gold $K\beta'$ peaks 96

9.2 Maximum available background region 99

9.3 Two- and pseudo-two-channel analysis 99

9.4 The peak to background ratio detection limit 101

9.5 System time constant and detector size 104

9.6 The gold detection limit 106

9.7 Discussion 107

10 QUANTITATIVE MEASUREMENT OF ROUGH ORE SAMPLES 111

10.1 Homogeneous concentrations 111

10.2 Thin layered sedimentary concentrations 113

10.3 Shape of the fluorescence sample 117

11 INSTRUMENTATION FOR THE GOLD ANALYSER 119

11.1 Instrumental requirements 119

11.2 Evolution of instrument 121

11.3 Components (block diagram) 123

12 CADMIUM-109 SOURCE AND COLLIMATOR 129

12.1 Production of Cd-109 129

12.2 Source and collimator design 134

12.2.1 Source window 137

12.2.2 Collimator shield 138

13 SAFETY ASPECTS 143

13.1 Liquid nitrogen 143

13.2 Intrinsic safety for fiery mines 146

13.3 Radiation safety 147

14 RESULTS OF THE FLUORESCENCE METHOD 153

14.1 Measurements at Leslie Gold Mine Ltd. 153

14.1.1 Equipment 153

14.1.2 Test site 154

14.1.3 Experimental 154

14.1.4 Details of the fluorescence measurements 155

14.1.5 Details of chip sampling and analysis 156

14.1.6 Comparison of XRF and chip sample values 158

14.1.7 Discussion 162

14.2 First prototype results from Marievale Gold Mine 165

14.2.1 Minimum length of stope face for quantitative estimation of the gold content at Marievale 170

14.3 Results obtained with the first prototype at Blyvooruitzicht Gold Mine 171

14.3.1 Results using the second prototype at Blyvooruitzicht Gold Mine 179

14.3.2 Minimum lenght of stope face at Blyvooruitzicht Mine for quantitative estimation of the gold value 184

15 CONCLUSIONS 186

REFERENCES 189

LIST OF TABLES

3.1 Potential radioisotopes for gold determination 26

7.1 Energy and relative intensity of the K X-rays of gold and lead 78

8.1 Effective non-extending processing times 87

9.1 Individual K X-ray lines of gold and lead 96

9.2 Spectral region and variances in gold ore analysis at various system resolutions 100

9.3 Data acquisition parameters in gold ore analysis for a typical 200mm^2 Ge detector at r=50kHz 103

12.1 Isotopes in the production of Cd-109 130

12.2 Absorption properties of shielding metals 139

14.1 Comparison of means of XRF and chip samples 158

14.2 Correlation between XRF and chip samples 160

14.3 Fluorescence measurements with the first prototype on 30 stope face sample at Marievale 166

14.4 Calculation of variances in the determination of gold concentrations at Marievale 168

14.5 Batch measurements at Blyvooruitzicht 173

14.6 Prototype 1 fluorescence and chip values and their correlation at Blyvooruitzicht 178

14.7 Prototype 2 fluorescence and chip values 180

14.8 Prototype 2 fluorescence measurements on 19 samples at Blyvooruitzicht 182

LIST OF FIGURES

3.1 Spectra of sources for gold K X-ray fluorescence 28

3.2 Angle required in incoherent scatterin to reduce energy of primary photon to 81 keV 30

4.1 Co-109 backscatter spectrum from blank 'rock' 33

4.2 photon interaction data for 'rock' 35

4.3 Shape of differential cross sections per unit solid angle for scattering of 88 kev photons from iron 36

4.4 Backscatter spectra from iron samples 39

4.5 Backscatter spectra from large sample of standard ore for different measuring geometries 43

4.6 Increase in backscatter intensity at 80 kev from peripheral sources relative to that from a central source 44

5.1 Linear detection efficiencies and their ratio vs. Ge detector thickness 48

5.2 Energy resolution of a 200mm^2 x 7mm Ge detector 52

6.1 Normalized Gaussian peak and background 57

6.2 General peak and background measurement 57

6.3 Single channel schemes for peak evaluation 60

6.4 Standardized background variances of R; background region unlimited 62

6.5 Standardized multichannel variances $^{m}V_{t_{max}}$ relative to $^{m}V_{\infty}$ 63

6.6a Minimum two channel variance in R 66

6.6b Discriminator positions in two channel analysis for minimum variance in R 66

6.7a Minimum pseudo two channel variance in R 67

6.7b Discriminator positions in pseudo two channel analysis for minimum variance in R 67

6.8a Minimum three channel variance in R 68

6.8b Discriminator positions in three channel analysis for minimum variance in R 68

7.1 Fluorescence spectra of standard gold ore sample 76

7.2 Fluorescence spectra of pure gold and lead 78

8.1 Analog pulse processing times 84

9.1 Discriminator positions for two channel evaluation of gold Kβ peaks 100

9.2 Measurement times for specified ratio detection limit vs. TC for various detector sizes 105

9.3 Minimum measurement times @ 250Hz/mm^2 vs. detector size 105

10.1 Edge-on fluorescence measurements of a 'sandwich' ore sample 115

10.2 Total count rate (>50keV) vs. probe to sample distance 116

11.1 First modular analyzer for in situ gold analysis 124

11.2 First prototype portable analyzer in use underground 124

11.3 Third prototype portable gold analyzer 125

11.4 Electronic block diagram of the third prototype gold analyzer 126

12.1 Cyclotron production yields of Cd-109 133

12.2 Source detector arrangement in the third prototype gold analyzer 136

14.1 Fluorescence and corresponding chip sample values from Leslie Gold Mine 159

14.2 Group means of fluorescence and chip values 160

14.3 Prototype 1 measurement error $(S_c^2 + S_g^2)^{0.5}$ 169

14.4 Length of face to be scanned at Marievale using prototype 1, to achieve a given precision in the given time 172

14.5 Comparison of batch and X-ray fluorescence estimates at Blyvooruitzicht 175

14.6 Bulk values of 152 batches at Blyvooruitzicht 176

14.7 Variogram of 152 consecutive batch values at Blyvooruitzicht 177

14.8 Length of face to be scanned at Blyvooruitzicht using prototype 2 to achieve the given precision in the given time 185

1 INTRODUCTION

The Witwatersrand geological system contains the world's largest known deposits of gold and it thus plays a major role in the economy of the Republic of South Africa. By the end of 1975 gold had accounted for approximately 66 percent of the total value of mineral products of the country from its earliest mining activities (Coetzee, 1976).

The depletion of ore reserves and ever increasing production costs have focussed attention upon the profitability of all aspects of gold mining. One of these, ore valuation, plays an important role in this. The great magnitude and the exceptional continuity of the Witwatersrand ore body make *in situ* evaluation of underground ore deposits feasible; at the low concentrations generally encountered evaluation from without the deep ore deposits would not allow anywhere near as high a precision of ore valuation.

The average mining depth is approximately 1,6 km below surface, approximately 75 Mt of ore are treated annually and the average grade of the ore treated is approximately 10g/t (10 parts per million).

1.1 Nature of the Witwatersrand gold deposit

The Witwatersrand gold ores were stratigraphically deposited in Precambrian times in successive cycles of sedimentation, with each cycle constituted by a varying

number of pulses of different intensity and character.

At present geological times, the planes of these tabular deposits are often almost horizontal, though they may be inclined at any angle up to the vertical and they have varying degrees of undulation and faulting. About sixty per cent of all gold ore is mined by explosive methods at a stoping (tabular excavation) width of less than one metre and the important heavy metal bearing conglomerate in these has a layer thickness or reef width of less than 200mm.

The gold bearing reefs are composed of a variety of quartz pebbles in a matrix consisting predominantly of quartz of sand size, with varying amounts of pyrite and other sulphides and some heavy minerals. The ore density averages 2,76t/m^3. Carbon is notable in some of the conglomerates. The gold occurs in the form of highly irregular particles ranging from 0,005 to 0,5mm across. The silver content of the metallic particles varies greatly - from less than 4 per cent to more than 32 per cent. (Coetzee, 1976).

The concentration of gold is at trace levels, the gold is thus seldom visible to the naked eye and other geological features commonly have to be relied upon for identification. The most prominent indicator is usually a reef band of pebble conglomerate; sometimes a carbon band or the separation of two geological layers, e.g. quartz and shale, serve as visual identification. These features are often not distinct and it is important to realize that although they are correlated with the gold concentration,

the correlation is poor. Discontinuities in the features and geological faulting and undulation augment the *in situ* problem of following the gold containing layer, and it is not uncommon that some mining is carried out on completely the wrong horizons, mistakes which can be rather costly particularly since the payable horizons missed may have become unmineable through this operation.

Uranium is often associated with the gold ores and the radiation from its decay products is sometimes used as a measurable indicator of the gold content, but the correlation is only medium to poor and uranium or radioactivity cannot be relied upon as primary indicator for gold without continued verification of the correlation.

1.2 Ore valuation

Ore valuation entails sampling of the ore body, determination of the mineral content of the samples, these two processes being referred to as evaluation of the ore, and assessment of the results to allow mining decisions to be made. In the valuation of three dimensional deposits only the position, mass and mass concentration of samples is required. Evaluation of samples of thin tabular deposits, however, entails the determination of mass of mineral per unit area. The dimensions of each sample thus need to be known so that the mass concentrations determined in the assay may be converted to the area concentration.

The conventional method of sampling (Storrar, 1977) in the gold mining industry has been chip sampling. At regular intervals of 3 to 10 metres in stopes, and at shorter intervals in development ends, delineating blocks, the rock

face (wall) is washed and dressed, i.e. cleared of loose pieces of rock and large steps, and the outline of the sample to be chipped is measured and marked off with crayon. A groove nominally 25mm or so deep and about 70 to 100mm or 150mm broad is chipped with hammer and chisel across the mineralized zone. For narrow reefs only a single sample of specified width (height) 80mm, 100mm or 150mm normal to the reef plane is cut if non-mineralized rock can be included in the upper and lower parts of the sample, otherwise the groove is lengthened to provide several samples. Between 0,5 to 2 kg of chippings are caught in a pan below the sample being taken. A rubber guard or a piece of cloth wound around the chisel near its point reduces the number of rock chips flying off.

Groove samples across tabular deposits, as far as possible should be of even depth, and rectangular in shape with solid square corners to allow simple conversion of mass- to area concentrations. The quartzites generally encountered in the Witwatersrand gold mines make this rather difficult in manual sampling and uneven friability across the mineralized zone can readily introduce sampling bias. Mechanical sampling with diamond wheel cutters offers only slight improvement at higher cost and inconvenience and, therefore, has limited application.

The highly erratic deposition of gold and the overall low values call for the area sampling ratio, i.e. the total projected area of the samples to that of the ore body, to be as large as possible, and for the samples to be representatively distributed throughout the ore body. The area sampling ratio and the distribution of

gold values determine the precision with which the value of a standard size ore body thathas been mined, or of one that is to be mined, may be assessed. In stope and development end chip sampling usually an area ratio of less than 0,0001 of the area mined is representatively sampled. A standard size ore body has not yet been stipulated and the required precision of valuation for this standard size for mining decisions frequently encountered still have to evolve; the precision of valuation can then be related to any size of ore body.

The main use of ore valuation from chip sampling has been for control of the grade of ore mined and to provide estimation of future ore reserves. Many mining decisions at present made on an arbitrary basis could benefit greatly from on improved precision in ore valuation. 'The maximun benefit (of ore valuation) is obtained from low grade areas as they become payable and the mining of areas is terminated as soon as possible after they become unpayable' (Johnston, 1973). The impending introduction of mechanisation into the gold mines will require much more concentrated mining for efficient use of the costly equipment. This will require a higher precision of valuation of ore bodies of the smallest sizes amenable to selective mining. A higher precision can be attained through better sampling continuity and a higher area sampling ratio usually at increased cost.

Other methods of underground sampling have been employed under particular situations to reduce valuation costs with varying degrees of success. Grab sampling of

broken ore is used in some mines, often in conjunction with chip sampling, for control of the grade of ore mined. For ore valuation the average stoping width of the area covered by a broken ore sample collection point needs to be known to allow conversion of mass- to area concentration. For narrow reefs a broken ore sample of 10 kg represents an area of the ore body similar to that of a chip sample of the order of 1 kg. It appears that even if the area sampling ratio of the ore body sampled is less than in chip sampling, the higher continuity feasible in broken ore sampling through reduced acquisition costs allows better representation of the parent ore body and thus improvement in valuation precision in some mining areas (Chelius, 1973). A limitation of broken ore sampling is that the smallest size of ore body that may be valued for selective mining is of the order of the total area covered by a sample collection point, i.e. usually one or more stopes.

Special bulk sampling, where 100% of the ore of a small area of an ore body is extracted and put through a sampling plant, has been used to obtain information for comparison with routine sampling results (Hallbauer, 1977), but this method precludes good sampling continuity for extended ore bodies.

The ore samples from underground are fed to a small jaw crusher and reduced to a certain size. The sample is then divided to reduce the amount and fed to a pulverizer where it is reduced to 100% -74μm. Fifteen to sixty grams of sample is placed in a fire-clay crucible and 80-90g of flux (Litharge 30%, Sodium carbonate 45%, Borax 25%, Maize meal

2g) is added. The crucible is placed in a reverberatory furnace at 1100°C, where the gold collects in a lead bead. The contents are then poured into a mould and cooled. The lead bead is removed and hammered into a cube and placed in a cupel in a muffle furnace. After about half an hour the lead has been absorbed and evaporated and the cupel is removed. The Au/Ag bead is weighed and the mass recorded. An average correction is normally applied for the silver content, the average being checked periodically. Although losses in the furnaces and during cupellation can cause errors (Wall et al., 1973), these errors are not serious in the evaluation of ores as sampling errors are dominant; they can, however, be important in the assaying of much lower concentration samples such as from tailings.

Usually the sample results are combined to obtain averages for valuation of stretches of ore for grade control and ore reserve calculations.

Improved geostatistical methods of valuation, dating from the 1950's (reviewed by Krige, 1964), have more recently been applied at a number of gold mines to control the quality of routine sampling and assaying and to provide realistic confidence limits in the ore valuation of any size of ore body.

The geostatistical methods are continuously being improved and it may be expected that the area sampling ratio, instead of being a stipulated value for a large section of a mine, will be able to be determined on a precise cost benefit basis according to the uses of the valuation and to the gold distributions encountered.

1.3 Alternative methods of evaluation of ores

The disadvantages of the conventional method of evaluation, where samples collected underground are assayed on surface, are the difficulty of unbiased chipping of samples from the narrow stope faces, the transportation of the samples to surface and the delay from the time of chipping until the results are available. Once in the laboratory the concentration of the samples can easily be determined by fire assay to high accuracy and precision.

Alternative laboratory methods of measuring the gold content, such as conventional X-ray fluorescence analysis, radioisotopic X-ray fluorescence analysis (Burkhalter et al., 1970), instrumental neutron activation analysis (Uken et al., 1966) and acid leaching, solvent extraction with atomic absorption spectrometry (Groenewald, 1969) have been investigated and were found to offer some advantages over fire assaying. However, to reduce the sampling problem in situ methods of evaluation of ore were considered.

Of the chemical methods chromatographic paint (Hallbauer, 1973) was shown to be useful in some qualitative investigations and while in situ chemical leaching or cyanidation (Lloyd et al., 1969) also has some potential, it is probably too time consuming for this application.

Instrumental methods for quantitative measurement of the gold content directly on unprepared stope faces were investigated. Although dispensing with arduous sample extraction and with preparation of the sample may seem very attractive, these methods face the problem of direct

physical measurement of trace concentrations of gold without any form of preconcentration with sophisticated equipment that needs to be carried through and operated in stopes. Furthermore even though an instrumental method may be used in rapid scanning of the whole stope face, thereby improving continuity of sampling over conventional periodic distance sampling, the depth of measurement into the rock face needs to be high enough so that also the area sampling ratio of the area of the ore body mined may be improved. For example chip sampling of sections 20mm deep and 100mm broad on a square grid pattern of 5m has an area sampling ratio of $20 \times 100mm^2 / 25m^2 = 0,00008$ whereas an instrumental method of scanning the whole stope face after similar 5m advances to a depth of only 0,1mm would have a poorer ratio of only 0,00002.

Measurement of gold values in narrow reefs directly on the stope face has the advantage over measuring gold values in broken rock in that the conglomerate is not diluted with waste rock and that there is no complicating factor of segregated broken sizes. The times to measure the same mass of rock to the same percentage precision are disproportionately longer for the lower average concentrations in the broken rock. Also, the surface of the rock to be measurred is somewhat less rough on the stope face than on the broken ore and the problem of controlling or correcting for a variable measuring geometry in quantitative sample evaluation is thus slightly reduced.

In considering the physical properties of gold which could be usefully applied in the design of a stope face

gold analyser, the entire electromagnetic spectrum had been reviewed. In the radio and microwave regions there appeared to be no properties of use; in the infra-red region the high reflectivity of metallic gold was noted; in the X-ray and gamma ray regions fluorescence and Mössbauer effects seemed potentially useful with electron excitation of X-rays a poor alternate; while in the heavy particle field, neutron activation showed some promise. Consideration of the thermal, electrical and magnetic properties did not reveal anything of interest.

Thus four physical, non-destructive methods appeared to be potentially useful.

Infrared reflectivity measurement with a 'vidicon' tube gave encouraging results (Hinde, 1971). This method, however, had three shortcomings: Optical resolution for the very fine gold particles was insufficient, only the surface of gold particles and not their mass could be directly assessed and the penetration into the rock is insufficient for the requirement of sampling a high ratio of the area of the ore body.

A closer assessment of the Mössbauer effect suggested that any method based on this effect would probably be impractical. It appeared that it would be neccessary to cool the rock to obtain the effect and that the rate of data acquisition would probably be too slow.

Gold K level X-ray fluorescence did, however, appear practicable and its development will be outlined in the next chapter.

The high cross section for resonance neutrons, the high

sensitivity of instrumental neutron activation analysis and the high penetration of neutron and gamma rays through rock had focussed much attention on this method. Laboratory investigations had been carried out at the National Institute for Metallurgy (Uken et al., 1966), and indications were that adequate sensitivity and rapidity could possibly be attained with gold ores. However, a high flux neutron source of californium-252 would be required and the difficulties of safe handling of such a source in a portable instrument in stopes seemed too great.

1.4 Discussion

To meet ever increasing mining costs defin[illegible] mprovements in the precision of ore valuation will be required. The conventional method of chip sampling offers little potential for improved evaluation of ores. Improvements in the laboratory analysis of samples can only have a minor effect on the evaluation because the main problems lie on the sampling side.

Bulk sampling of broken ore appears to alleviate the sampling situation in some mines under present mining conditions, but the area selectivity and degree of improvement will be insufficient for future demands.

It was realized that only by rapid scanning of exposed stope faces to a depth of more than a millimetre could the continuity and area sampling ratio be improved sufficiently for selective mining to a scale smaller than the size of present day stopes. The important criterion was that as much rock as possible should be measured per unit time to an acceptable measurement precision.

The underground environment where ores have to be evaluated is fairly harsh for a sophisticated instrument that is usually operated in an air conditioned laboratory. The industry average wet bulb temperature in working stopes is about 29°C and average wet Kata readings are about 11,5. Working height is often restricted to less than one metre because of broken rock lying in working places, and instruments may have to be dragged across this highly abrasive quartzite. Air velocity averages 1m/s and the air may be dusty. Illumination is by caplamp. Ore evaluation is sometimes required in non-working places and in these places conditions may be considerably poorer.

A number of potential instrumental methods were considered for direct quantitative measurement of the gold content in the rock without having to remove a sample from the stope face. Careful preparation of the sample surface also was to be avoided as this would defeat the object of not having to take a sample. Only penetrating radiation has the potential of increasing the area sampling ratio. Of the instrumental methods only radioisotope excited K level X-ray fluorescence of gold and detection of the radiation with a high resolution solid state detector appeared to be within reach of present day technology for this application.

The term gamma ray fluorescence is used in this work to distinguish the method from conventional X-ray fluorescence analysis. The energy region used for excitation and measurement falls above the energy region conventionally used in X-ray fluorescence analysis and at the lower end of conventional gamma ray specrometry: Gamma radiation is used

for excitation and the high energy gold K X-rays are detected. A 'low energy' photon detector suitable for this intermediate or transitional energy region is employed. Both the disciplines of gamma ray spectrometry and of X-ray spectrometry are merged in this application.

To achieve an acceptable rate of rock analysis all the parameters of excitation, detection and data processing had to be optimised for a portable instrument to be used in the hostile stope environment. In the following chapters, after an outline of the method, the various parameters critical to the method are discussed and developed from fundamental principles as the empirical approximations most commonly employed in both disciplines were not amenable to the rigorous treatment and would not have permitted an indication of the maximum improvement possible on a given combination of parameters. Some early underground sample evaluations taken with prototype instruments are presented to illustrate the introduction of gamma ray fluorescence analysis into ore valuation of the Witwatersrand gold deposits.

2 OUTLINE OF THE DEVELOPMENT OF THE FLUORESCENCE METHOD

The *in situ* instrumental evaluation of gold ores is a sophisticated task involving a large number of aspects. These may be considered as a chain of parameters that need to be optimised as a whole. Some of the parameters may be considered almost independently of each other while the dependence on others calls for a compromise, yet weakness of any one parameter results in poor overall performance while excessive strength in another may simply be wasteful.

The aspects that needed consideration were the nature of the ore deposit on both a large scale and a microscopic scale, the requirements for ore valuation, the environment for the evaluation, the human aspects of *in situ* instrumental operation and operational procedure, operational safety, a series of measurement and instrumental parameters, measurement interferences and the presentation and utilization of measurement data.

It was mentioned in the opening chapter that most of the gold occurs in very narrow deposits and in a wide range of particle sizes, and that the ratio of the area sampled to the area mined needs to be higher than the area ratio hitherto employed with chip sampling if the precision of ore valuation is to be improved.

2.1 Rock penetration for an instrumental method

The effective depth of measurement in rock of a potential

instrumental method would have to be an improvement on the maximum effective depth of current chip sampling. This is nominally a 20mm deep cut of 100mm length made every 5 metres of an exposed stope face; if this projected area were spread out evenly along the stope face from one cut to the next, the effective depth of sampling would be 20mmx100mm/5m=0,2mm. The sizes of gold particles found in the reef require that also the measurement depth in gold be sufficient to penetrate the larger gold particles. If only a thin surface layer of the larger gold particles could be penetrated then the projected area of the particles, rather than their mass would be reflected in the measurement values.

The narrowness of most of the gold bearing ore layers needs to be taken into account when considering large penetration depths. In the edge-on measurement of a narrow layer of gold bearing ore the absolute concentration in the sample to be measured decreases as the sample dimension normal to the layer increases beyond the layer thickness, thus including waste rock in the sample. Because the gold concentrations that have to be determined are at trace levels, the measurement phenomenon to be detected manifests itself only weakly and it is therefore advantageous not to include much waste rock in the sample so that the phenomenon may appear relatively stronger. A high efficiency in the utilization of measuring radiation is desirable for such a weak phenomenon and this can be attained only with an uncollimated or wide-angle measurement geometry. With this geometry the measurement penetration should ideally be similar in value to the ore layer thickness and the

measuring head should be a similar distance away from the sample surface. This would indicate an optimum rock penetration depth of a few millimetres for most of the Witwatersrand deposits, but this would be impractical. There would be no point in employing a method with an effective sample penetration depth less than about 20mm, as it would be difficult to discern a layer and to guide a small measuring head, in scanning rapidly along a rough stope face, with a precision better than this.

From a penetration and concentration point of view the gamma-ray excited, gold K X-ray fluorescence method is thus ideal for the evaluation of most of the Witwatersrand gold deposits: the gold K X-rays have a half-range in rock of 13mm, i.e. they lose half of their intensity in going through 13mm of rock, and any exciting gamma radiation for these X-rays has a half-range in quartzite longer than this. In solid gold the half-ranges of gold K X-rays and of exciting gamma rays are respectively 0,2mm and greater than 0,04mm, thus most of the larger gold particles that may be encountered are easily penetrated so that the mass of gold particles, rather than their surface area is represented in the fluorescence measurement.

2.2 Description of the fluorescence system

Gamma radiation from a radioisotope source is used to excite the characteristic K X-rays of gold in a stope face sample. These in turn are detected by a germanium detector and the detector signals are processed to give a quantitative indication of the gold concentration.

Cadmium-109 emits 88 keV gamma rays which can be efficiently absorbed by the K electrons of gold which are then emitted with that energy less their K-shell binding energy of 80.7 keV, i.e. as 7 keV electrons. The vacant gold K atomic shell is subsequently filled with an electron from the L, M or N shell and in this process may isotropically emit a fluorescent gold K X-ray.

The 88 keV gamma rays are also scattered in all directions by electrons in the rock matrix. In the coherent scattering process the energy of the incoming and outgoing photon remains unchanged whereas in the incoherent scattering process some energy is lost to an electron. The probabilities of scattering in a given direction vary with the scattering angle and are different for the two types of scattering . Whereas the gold fluorescence X-ray spectrum is the same in all directions (except for differences from absorption through the matrix), the matrix scatter spectrum has different profiles at different scattering angles. Cadmium-109 was chosen primarily because its 88 keV photons excite gold efficiently while at close to a 180° scattering angle the scattering spectrum has a very low intensity in the region of the gold K X-rays.

A miniature point source in combination with a wide angle tungsten collimator shield was developed for mounting concentrically in front of a germanium detector so that a source-sample-detector scattering angle close to 180° could be achieved in all forward directions of the source-detector probe even for sample to probe distances as short as 25mm.

The 22 keV silver X-rays, emitted abundantly by

Cadmium-109, were filtered out to reduce the potential radiation hazard and so as not to take up any useful count rate handling capability of the detection and analysing system.

A hyperpure germanium photon detector, cooled by liquid nitrogen, was specified because of its high energy resolution and efficiency for photons in the gold Kβ X-ray energy region. The size of 200mm^{2}x7mm deep was evaluated for optimum data acquisition rates.

Instead of relying on conventional empirical approximations for spectrum evaluation, a fundamental study was undertaken to allow quantitative comparison of different methods of spectrum evaluation. An optimised single channel scheme for the two correlated gold Kβ′ peaks was developed on this foundation. This provides efficient spectrum evaluation with instrumental simplicity needed in a portable instrument.

Two important developments for quantitative in situ gold determination were i) the derivation of a method of ratioing the measured gold peaks and their immediate background to cope with the variable geometry measurement of rough surfaces, and ii) for conversion of mass to area concentration a method of feedback to control the probe to sample separation within predetermined limits. In the latter method the total spectrum count rate is interpreted as a probe to sample distance, the rate is continually displayed to the operator to guide him for human servo control of the distance and the rate is internally monitored to inhibit data acquisition when the rate is not within set limits i.e.

when the measuring geometry is not within corresponding distance limits. A South African patent (Rolle, 1974) and a United States patent (Rolle, 1977) were granted for this concept.

The basic concepts of extending and non-extending processing times in the analog processing of random signals were developed together with new concepts of pileup parameters to allow a quantitative description of the data acquisition rate of a complete analog pulse processing system. With this foundation the pulse processing times could be optimised for given detector resolution parameters to maximize the non-piled up data acquisition rate.

Digital data processing was trimmed to the simplest system that could automatically provide data in calibrated concentration units to the operator and for storage in an internal data memory for retrieval above ground. More sophisticated, microprocessor-based systems can, however, be expected in the near future.

The layout of the portable system was designed for maximum operational simplicity and operator convenience, particularly for rapid scanning of long stretches of stope face.

The instruments so far tested underground have developed from a stationary, mains-operated model through three prototype versions of portable instruments. At the close of the writing of this thesis a number of instruments of the third prototype were in the stages of accumulating data in ore valuation field trials at various mines.

3 EXCITATION OF FLUORESCENT X-RAYS

For the determination of trace amounts of a heavy metal in a light matrix by XRF spectometry, it is necessary to choose a source which will excite the X-rays of interest as efficiently as possible. However, efficiency of excitation is not the sole criterion, because the excited X-rays must be detected against a background signal caused by the scattering of photons by the matrix or by photons in the source of energies other than those which excite the fluorescent X-rays most efficeintly. Accordingly the source of exciting radiation must be chosen not only on the grounds of the efficiency of excitation, but also so that it may minimize the background radiation seen by the detector. Excessive background radiation can reduce the efficiency of the detection system, increase the potential radiation hazard, and may reduce the signal-to-noise ratio in the energy regions in which the fluorescent X-rays of interest occur.

In what follows, therefore, all possible means for exciting the gold K and L X-rays are considered first, and then the various potential sources for K level excitation are compared not only on the grounds of the efficiency with which they can excite these X-rays, but also on grounds of the reduction in the total flux received by the spectrometer; the maximisation of the signal-to-noise ratio in the energy region of interest; and the practicability of

the various types of source when used in a portable underground instrument, which is the ultimate intended practical outcome of this work.

3.1 Particle induced X-ray emission

For X-rays below about 5 to 15 keV ($1eV=1,602x10^{-19}J$), charged particle excitation, e.g. by means of protons or alpha particles, offers good fluorescence cross sections while producing a relatively low scatter background in the recorded X-ray spectrum. Excitation cross sections of charged particles in the 1 to 50 MeV range lie in the region of 0,1 to $1m^2/kg$ which is comparable with that for photon excitation. The bremsstrahlung intensity depends on the square of the charge (z) per mass (m) of the incident particle i.e. on $(z/m)^2$ so that, with proton or alpha excitation as compared with direct electron excitation, problems of the associated background in the recorded spectrum are reduced by the order of the square of the proton/electron mass ratio. Charged particle excitation has, however, three drawbacks:-

i) their range in air is limited;

ii) apart from alpha particles emitted during radioactive decay, they have to be produced in accelerating machines and thus are unlikely to be practical underground and iii) secondary electrons are emitted and may result in an increase of the relevant background.

3.2 Photon excitation

In the past it was found that for X-rays above 5 to 15 keV, photon excitation offered superior detection limits (Woldseth, 1973).

The fluorescence excitation efficiency of photons of energy E decreases approximately as E^{-3} above the X-ray absorption edge of the element, i.e. 80,7 keV for the gold K level. Photons of energy below the absorption edge cannot excite the relevant group of X-rays.

Photon sources can be classified into three main groups depending on the mode of production of the principal radiation emitted, namely bremsstrahlung- , X-ray- and low energy gamma sources.

3.2.1 Bremsstrahlung sources

Bremsstrahlung is produced by the deceleration (or acceleration) of electrons. X-ray tubes for XRF are essentially operated as bremsstrahlung sources. The photon spectrum is continuous up to the maximum of the electron energy. The continuum spectrum is suitable for the simultaneous excitation of a whole range of elements but is not optimised for any particular element.

3.2.2 X-ray sources

Primary X-radiation is produced by atoms ionized through electron bombardment, nuclear recoil or internal conversion.

The photon spectrum consists of a group of characteristic X-ray lines which may be particularly suited for the selective excitation of some individual element. If a certain interfering element is to be discriminated against, then a filter, or a secondary target of either that element or one of slightly higher atomic number Z, may be placed in the primary photon beam. This can remove all radiation capable of exciting the interfering element,

partially converting it to X-rays of energies more efficient in exciting still lower-Z elements, thus allowing these to be selectively excited. More efficient use of radiation is, however, made by excitation with direct primary radiation.

In a well-designed, low energy source the intensity of the group of X-ray lines may constitute 90% of the total radiation from that source. At higher energies, scattering effects are relatively more important, and typically only 30 to 60% of the total radiation appears as the X-rays of interest.

3.2.3 Low energy gamma sources

Gamma radiation is produced in the decay of excited nuclear states to lower states of the nucleus. Most radioisotope decay schemes are complex and involve several gamma energies usually initiated by a charged particle. However, some decay schemes are simple with practically no charged particle emission and only one or two gamma energies, or all but the energy transitions of interest are of very low intensity.

Gamma sources for XRF are potentially monoenergetic sources that can give optimum excitation for individual elements.

A near perfect gamma source for XRF excitation of a particular element would exhibit the following characteristics -

a) decay by electron capture (EC) or isomeric transition (IT) with little internal conversion; other modes of decay are accompanied by a bremsstrahlung

continuum and internal conversion reduces the intensity while producing unwanted X-rays.

b) an intense gamma transition near the absorption edge of the element of interest with no high energy gammas. The high energy radiation increases background in the detected spectrum and aggravates radiation problems.

c) a sufficiently long halflife to obviate the need for frequent calibration of the instrument and replacement of the source.

d) an acceptable production cost - most of these isotopes are accelerator-produced and thus costly.

Gamma-ray sources are particularly convenient for the excitation of the high energy X-rays of the heavy elements.

3.3 Comparison of X-ray tubes and radioisotope sources

The primary advantage of X-ray tubes is the availability of a flux having an intensity orders of magnitude greater than is produced by radioisotope sources. The versatility of a tube through choice of operating conditions, and the simple fact that a tube with its potential radiation hazard, can be switched off, are secondary advantages.

Radioisotope sources have the advantage of being lightweight, having a very stable, predictable output and offering simple high energy XRF excitation.

3.4 Radioisotope sources for excitation of gold K X-rays

The gold K absorption edge lies at 80,7 keV and only source photons of higher energy will excite the K X-rays effectively.

3.4.1 Primary emissions of potential radioisotopes

A number of potential radioisotopes and their primary radiations are listed in Table 3.1. The probability of producing a primary photon of particular energy during the decay of an atom depends on the decay scheme and often is not 100%. Furthermore the primary photon may be internally converted without emerging from the atom. The percentages in the fifth and sixth columns of Table 3.1 refer to the number of atoms decayed. Percentages above 100% are feasible from complex decay schemes and consecutive decays. The photoelectric cross section μ_{ph} for K level excitation is $0,71 m^2/kg$ Au for photons barely exceeding 80,7 keV. As the photon energy E increases, the excitation efficiency decreases approximately as E^{-3}, and the parameter $(E/80,7)^{-3}$, with E in keV, shown in the 7th column of Table 3.1 is an indication of the gold K-level excitation efficiency of the primary emission relative to that of 80,7 keV photons.

3.4.2 Secondary emissions from sources

If the radioisotopes could be mounted on a thin film then only the primary radiation would be observed. For practical applications the radioisotopes need to be encapsulated and shielded from the detector. Besides the primary radiation the source spectrum therefore contains X-rays and scatter peaks from the source backing and window and from the source material. The source scatter peaks are relatively small because the heavy metal backings, such as Ta and W used in these applications, attenuate photons in the 80 to 200 keV region predominantly by photoelectric absorption. At these

Table 3.1 Potential radioisotopes for gold determination

ISOTOPE	HALF LIFE days	DECAY MODE	PRINCIPAL PHOTONS keV	INT. CONV. %	EMISSION %	REL.EXCIT. EFFICIENCY (max)
Ba-133	2628	EC	81*	57	34	0,99 (1)+
			356	2	62	0,01 (0,16)
			276;303;384	1	25	0,02 (0,2)
			54;80;160	12	5	0,09 (0,55)
Tm-170	128	$\bar{\beta}$	84	21	3,4	0,88 (1)
			brems(968)			0,00 (1)
Cd-109	453	EC	88	96	3,8	0,77 (1)
			AgKX 22;25		102	0
Gd-153	241	EC	97	8	30	0,57 (1)
			103	30	20	0,48 (1)
			70	11	3	0
			EuKX 41;47		110	0
Co-57	271	EC	122	1	85	0,29 (0,94)
			136	1	11	0,21 (0,75)
			14		9	0
			FeKX 6,4;7		55	0
Te-123m	120	IT	159		83	0,13 (0,56)
			TeKX 27;31		50	0
Pm-147	957	$\bar{\beta}$	brems(225)		50	0,05 (1)
			target PbX		<1	0,56 (1)
Ce-139	140	EC	166	20	80	0,12 (0,52)

* underlining indicates the photon of interest

\+ figures in brackets indicate the maximum relative excitation efficiency after incoherent scattering through an optimum angle

energies the usable primary radiation emitted from a source may thus constitute 50% or less of the total radiation.

Typical source spectra measured with a hyperpure Ge detector are shown in Figure 3.1.

3.4.3 The excitation spectrum in thick samples

For gold determination in a light geological matrix the excitation spectrum above 81 keV needs to be considered.

Photons at these energies are predominantly scattered, with less than 20% being photoelectrically absorbed. In a 'thin' sample the scattered radiation leaves the sample but in a 'thick' sample this radiation is available for further interaction with the sample.

Above 81 keV, scattering in a light matrix is largely incoherent so that inside a sample not only the intensity of the exciting radiation diminishes exponentially with depth, but the energy of the radiation is lowered as well. The energy E' of a photon scattered from a free electron at rest is a function of the scattering angle Θ and the incident photon energy E. It is given by the Compton (1923) equation for conservation of momentum and energy

$$E' = E/[\ 1 + (1-\cos\Theta)E/(mc^2)\ ]$$

The maximum angle through which a photon may be incoherently scattered before its energy is reduced below that required for the excitation gold K X-rays (81 keV) is shown in Figure 3.2. The reduction in the energy of an incoherently scattered photon, if it is still above 81 keV, results in an enhanced efficiency for the excitation of gold. The maximum relative efficiency for Au K-level

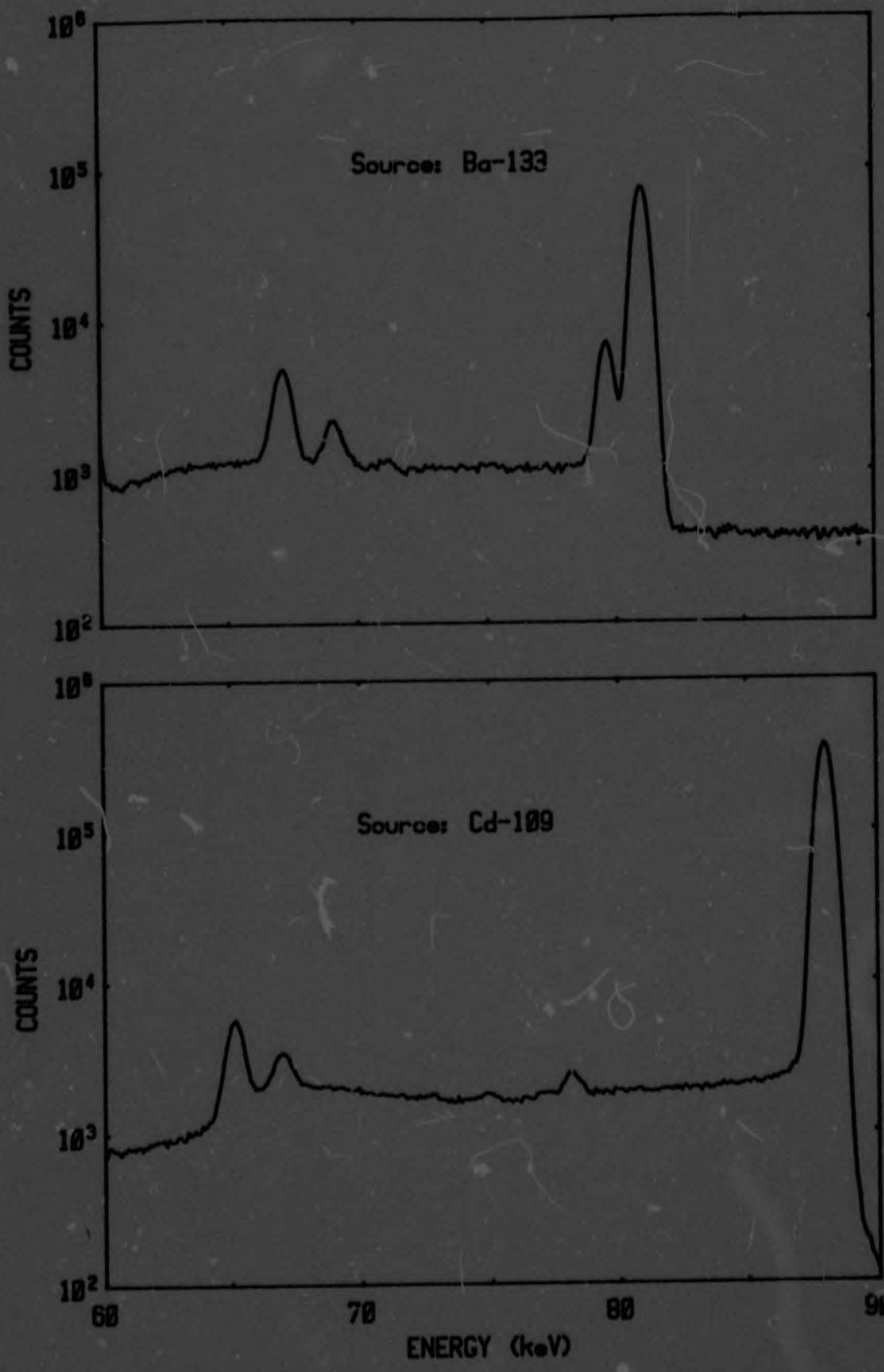


Fig. 3.1 Spectra of sources for gold K X-ray fluorescence

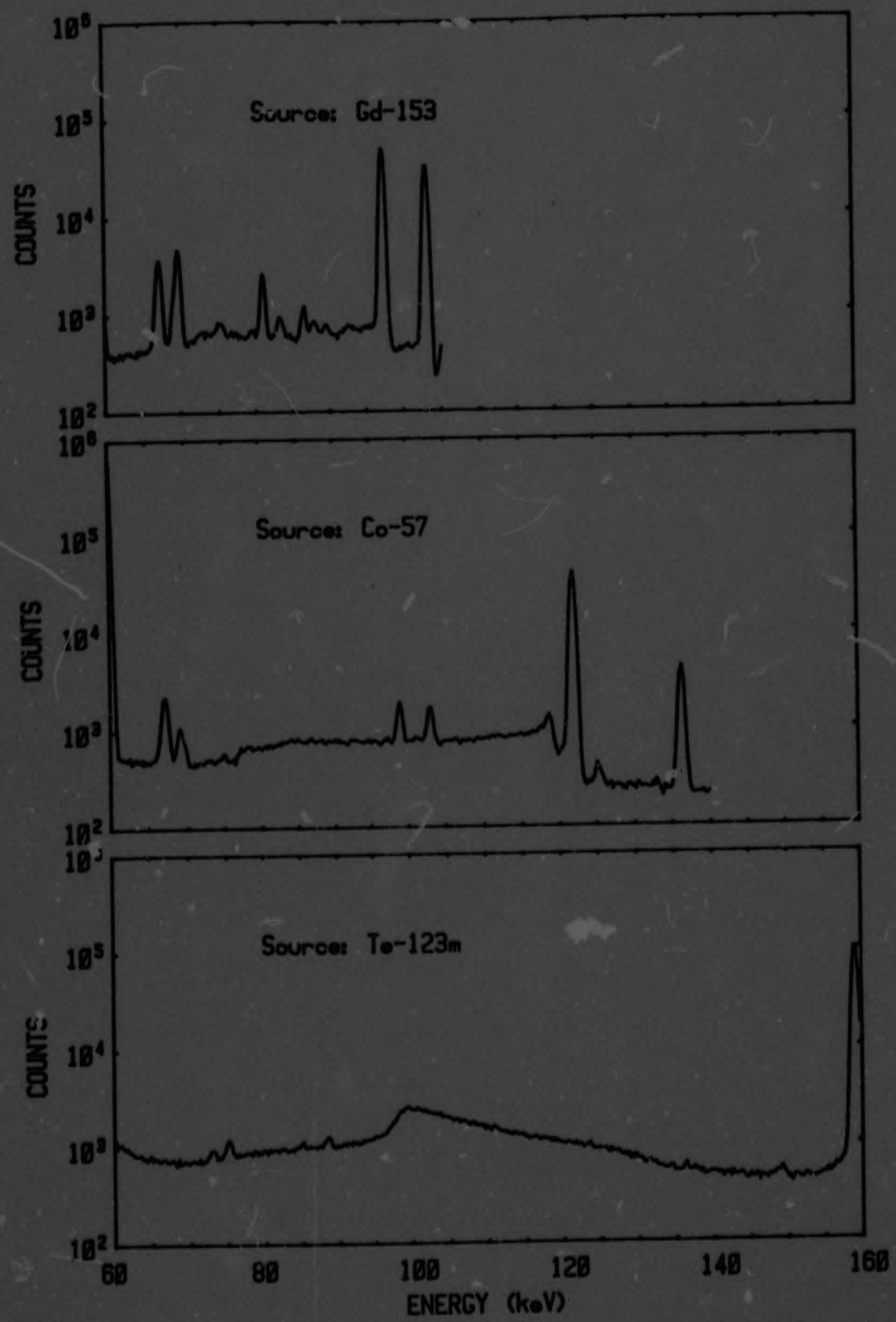


Fig. 3.1 (continued)

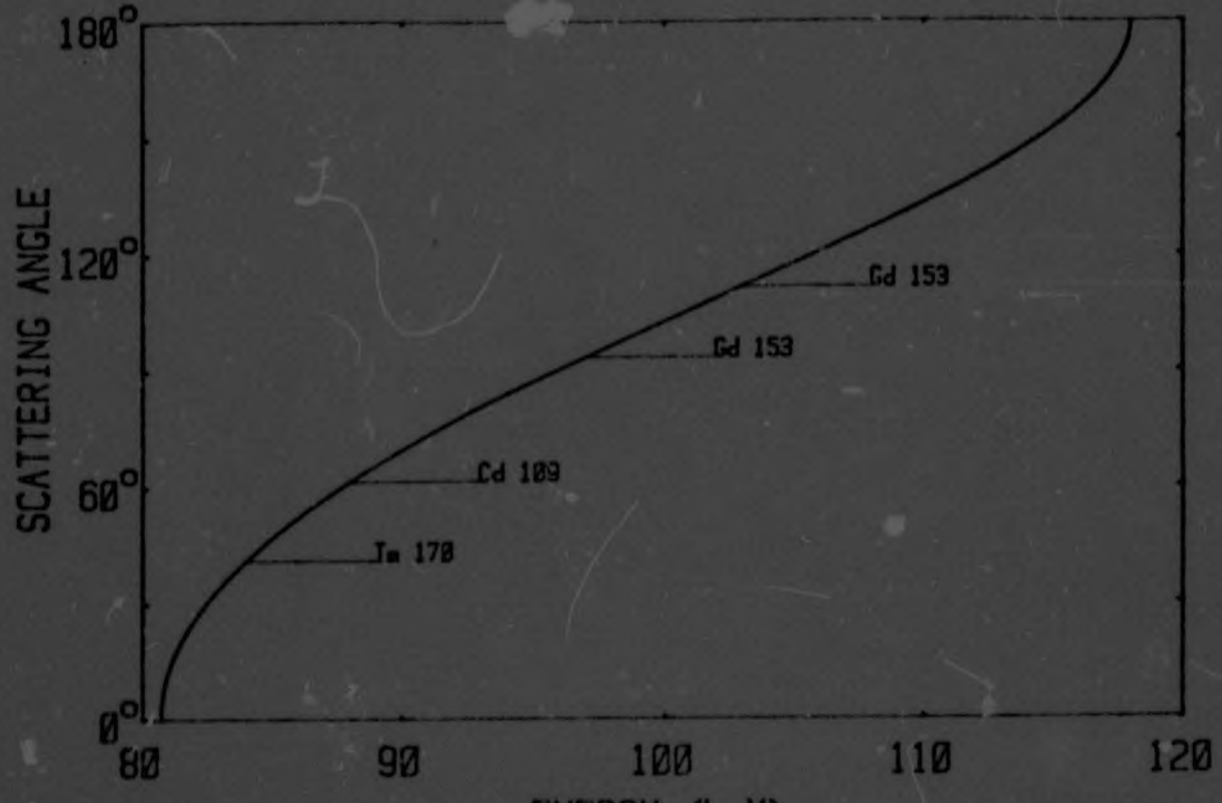


Fig. 3.2 Angle required in incoherent scattering to reduce energy of primary photon to 81 keV

excitation of singly scattered photons is given in parentheses in Table 3.1. This is analogous to the enhancement effect in XRF at lower energies, except that there, instead of being geometry dependent, it depends on the presence in the matrix of elements of atomic number Z a little higher than of the element of interest, because the effect occurs through fluorescence. The average excitation efficiency in a thick sample lies between the two values given in the table; multiple scattering, sample depth dependence and measuring geometry dependence as well as variations in matrix composition make precise calculation difficult.

In an 'infinitely' thick sample, photons scattered in a

forward direction remain in the sample for further interaction but those scattered backward have a lower probability of further interaction because they may also leave the sample. During scattering, the photons are polarized, and from the second scattering event, a photon tends to be focused to the plane defined by the first event, thus, compared to independent processes, the probability that a multiply scattered photon may leave the sample is enhanced.

3.4.4 Excitation of other heavy elements

X-rays of other heavy elements could possibly interfere with the measurement of trace amounts of gold. Elements from hafnium to radon have K X-rays in the vicinity of the gold X-rays. Only lead has a significant concentration among the heavy metals in Witwatersrand gold ores. All the sources listed in Table 3.1 can excite lead X-rays. At the start of this investigation the reported energy of 87,7 keV for the Cd-109 gamma transition (Lederer,1967) indicated that lead with a K absorption edge of 88,0 keV would not be excited, but experiments soon showed very efficient excitation of this element, and subsequently the gamma energy was reported at 88,023 keV (Dragun,1976).

Uranium is an economically important element associated with gold. Its K absorption edge lies at 115,6 keV. For direct excitation of U only sources emitting photons of energy higher than this can be used.

Measurement of lead, a decay product of uranium, may prove to be a useful measurement for uranium valuation in the Witwatersrand deposits where hardly any leaching is

forward direction remain in the sample for further interaction but those scattered backward have a lower probability of further interaction because they may also leave the sample. During scattering, the photons are polarized, and from the second scattering event, a photon tends to be focused to the plane defined by the first event, thus, compared to independent processes, the probability that a multiply scattered photon may leave the sample is enhanced.

3.4.4 Excitation of other heavy elements

X-rays of other heavy elements could possibly interfere with the measurement of trace amounts of gold. Elements from hafnium to radon have K X-rays in the vicinity of the gold X-rays. Only lead has a significant concentration among the heavy metals in Witwatersrand gold ores. All the sources listed in Table 3.1 can excite lead X-rays. At the start of this investigation the reported energy of 87,7 keV for the Cd-109 gamma transition (Lederer,1967) indicated that lead with a K absorption edge of 88,0 keV would not be excited, but experiments soon showed very efficient excitation of this element, and subsequently the gamma energy was reported at 88,023 keV (Dragun,1976).

Uranium is an economically important element associated with gold. Its K absorption edge lies at 115,6 keV. For direct excitation of U only sources emitting photons of energy higher than this can be used.

Measurement of lead, a decay product of uranium, may prove to be a useful measurement for uranium valuation in the Witwatersrand deposits where hardly any leaching is

thought to have taken place.

Excitation of the platinum group metals is very similar to that of gold and the same sources can, therefore, be considered for their determination in ores.

Good shielding materials are by their nature efficiently excited and possible interference by these X-rays needs to be held to acceptably low levels.

4 THE BACKGROUND SPECTRUM

A spectrum of 88 keV Cd-109 radiation backscattered from a blank rock is shown in Figure 4.1. It was measured with a system resolution of 600eV full width half maximum (FWHM) at 88 keV and the scattering angle from source to sample to detector was greater than 165°. Direct radiation from the source or source shield to the detector was negligible.

The most prominent feature in the spectrum is the intense incoherent or Compton scattered peak C. A much smaller peak marked A, approximately 1/100 of the peak

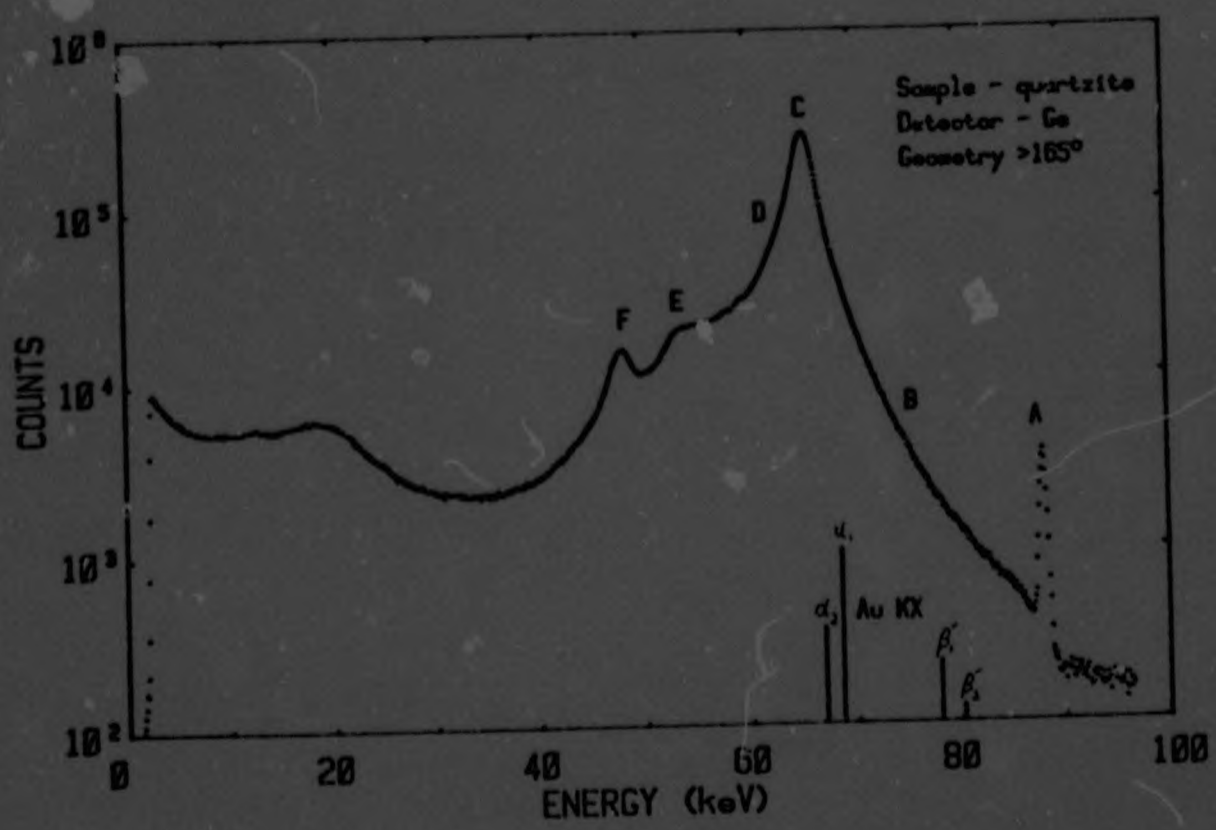


Fig. 4.1 Cd 109 backscatter spectrum from blank rock

intensity of C, arises from coherent scattering of the 88 keV source radiation. Peaks E and F are tungsten K X-rays from the source shield, backscattered by the sample. Our main concern is with the continuum region B where the gold K X-rays have to be measured or with region D when higher energy sources are used for which the prominent Compton peak C lies above the energy of the gold K X-rays.

The true sample spectrum is degraded by the resolution of the detection system so that sharp lines appear in the recorded spectrum as narrow Gaussian peaks of specific width. Minor, usually insignificant, deviations from a perfect Gaussian shape occur as a result of imperfections of the system.

The background under a peak determines the detection limit for the peak, and the total background flux taxes the pulse handling capability of the measuring system, thus limiting the speed with which a detection limit can be attained.

An understanding of the scattering processes is important if possible optimisation of the background spectrum is contemplated.

4.1 Photon scattering

Quartz with up to 5% pyrite may be considered the typical matrix for Witwatersrand gold-bearing conglomerate. The relevant photon interaction data, adapted from Gwozdz et.al.(1973), for SiO_2 and SiO_2 + 5% Fe_2O_3 are plotted vs. energy in Figure 4.2. Below 50 keV photoelectric absorption is the dominant mechanism for the attenuation of the photon intensity. Scattering here has a much lower

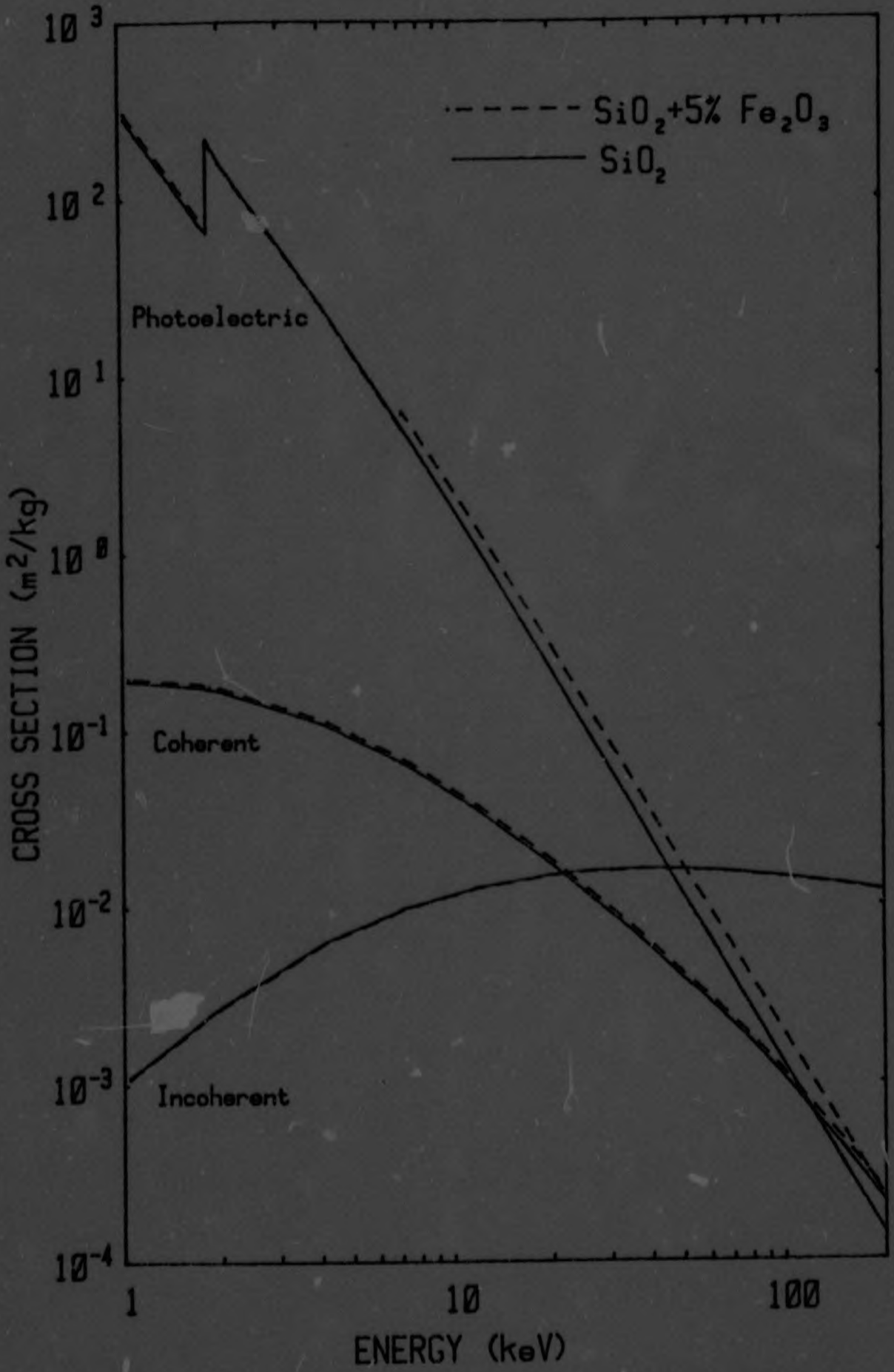
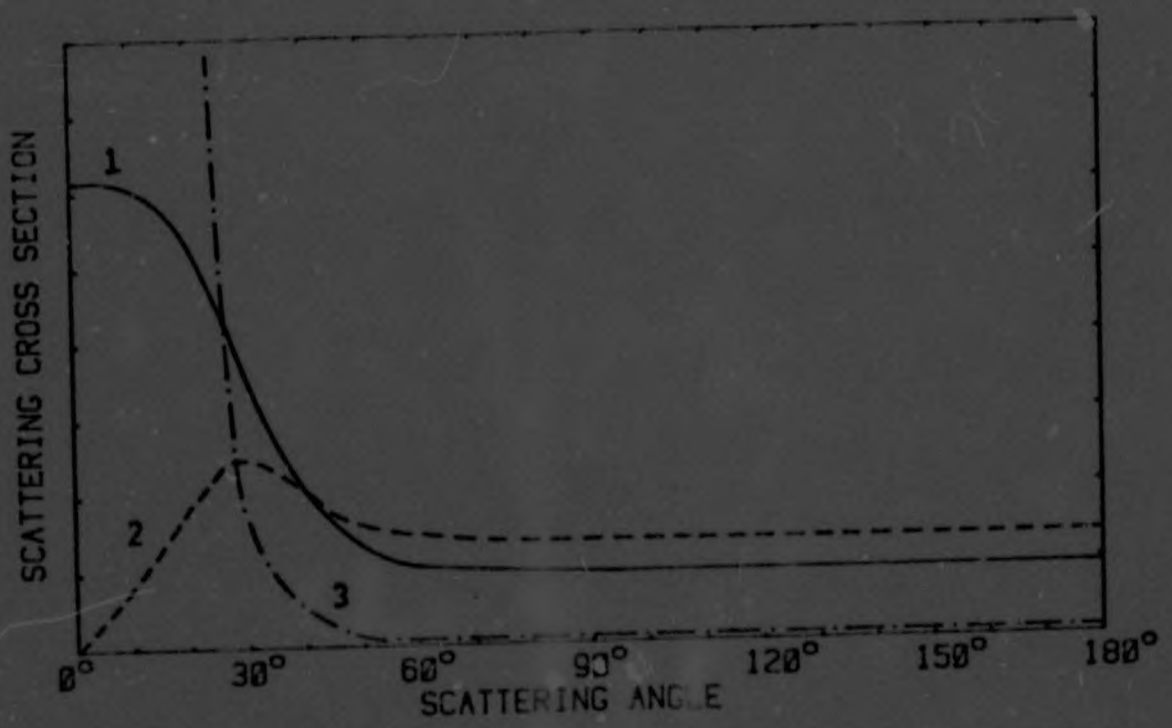


Fig. 4.2 Photon interaction data for 'rock'



4.2 Shape of differential cross sections per unit solid angle for scattering of 88 keV photons from iron. (1)-Compton free electrons, (2)-incoherent and (3)-coherent (after Davisson, 1968).

probability so that the background is low relative to the intensity of the X-ray peaks. Furthermore, the background spectrum below about 20 keV resembles that of the source radiation because scattering here occurs essentially coherently, i.e. without energy loss. The major attenuation of the photon intensity in the energy region above 50 keV comes from the incoherent scattering effect. At 80 keV the coherent scattering cross section is smaller by a factor of 7 or more. The energy loss in this incoherent scattering process results in a translation of the source radiation spectrum to lower energies and considerable modification of this spectrum.

Whereas fluorescent X-rays are emitted in all directions with equal probability, scattering of photons is

anisotropic. The cross sections shown in Figure 4.2 are the values integrated over all directions. The recorded background is thus dependent on the measuring geometry.

The energy dependence on scattering angle θ for a Compton electron (i.e. stationary electron) was given in 3.4.3 -

$$E' = E/[\ 1 + (1 - \cos\theta)E/(mc^2)\ ]$$

Klein and Nishina (1929) derived the cross sections in Compton scattering. The differential cross section per unit solid angle is illustrated for iron in Figure 4.3 for unpolarized 88 keV photons.

Bound electrons have specific momentum, and for incoherent scattering at a given angle the photons have an energy distribution known as the Compton profile. Only the peak energy corresponds to the above scattered energy equation. Compton profiles have been calculated from atomic wave functions (Clementi, 1965) and have been measured for a number of gases by Eisenberger et al.(1972). Most of the intensity in regions B and D of Figure 4.1 can be accounted for as the Compton profile. Some of the intensity, however, results from multiple scattering (discussed in the next section) and from instrumental pulse pileup discussed in chapter 9.

Coherent scattering would not be possible from unbound electrons. The peak A at 88 keV in Fig.4.1 is clear evidence that 88 keV photons can be scattered coherently through angles $>165^{o}$ by elements in the sample whose electrons have binding energies well below 10 keV.

An interesting feature of the scattering cross sections

is illustrated in the spectra for photons scattered from iron shown in Figure 4.4. There is a marked step about 7 keV below the 88 keV excitation energy - this energy difference corresponds exactly to the Fe K electron binding energy. The incoherent cross section drops sharply in favour of coherent scattering for energy transfers lower than the binding energy. This is shown qualitatively in Figure 4.3, in which the variation of differential cross sections with unit solid angle is given. A variable iron concentration would result in a variable step in the background spectrum at 81 keV and would reduce the precision with which the background in the gold Kβ peak region could be determined. The percentage of pyrite in Witwatersrand gold bearing conglomerates is, however, low and can cause only a very small step. Furthermore the intensity in the spectral region affected by the step forms only a small fraction of the background intensity useful for the evaluation of the gold Kβ′ peaks so that deterioration in precision would hardly be noticeable in this application.

4.2 Scattering spectrum from thick samples

In thick samples additional intensity in the spectral region between the coherent and Compton peaks arises from incoherent followed by coherent scattering, or vice versa. The incoherent process changes the energy of the photon with a corresponding change in scattering angle which may be insufficient for the photon to return to the detector and the coherent process further changes the direction so that the photon may reach the detector.

The process of combined coherent and incoherent

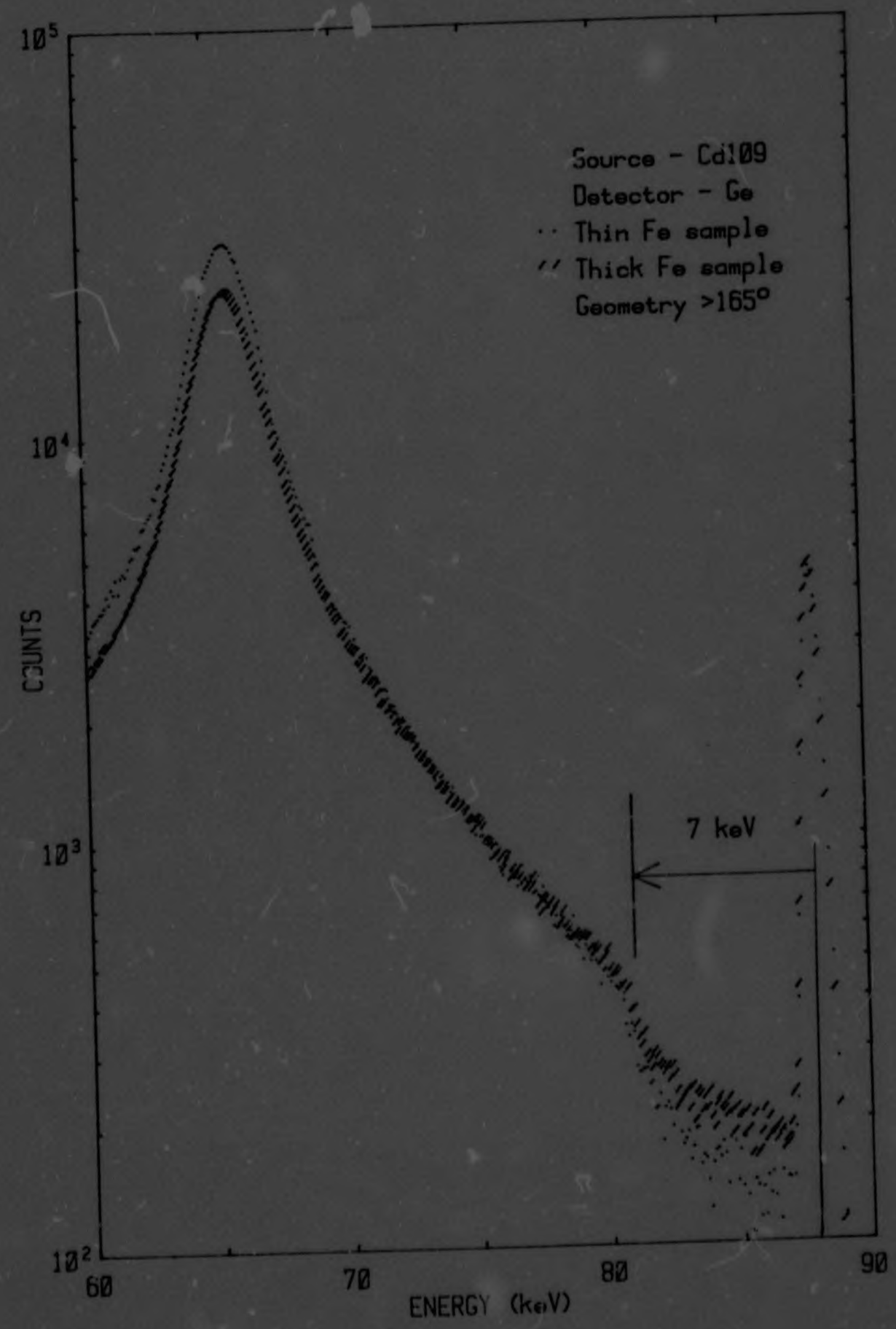


Fig. 4.4 Backscatter spectra from iron samples

scattering in thick samples is confirmed by the relative intensities of the superimposed spectra in Fig.4.4. These have been normalized to the same 88 keV integral peak intensity. The 'thin' sample consisted of a single disc 25mm diameter, 0,5mm thickness; the 'thick' sample consisted of 40 similar discs stacked behind the 'thin' sample. The intensity slightly below 88 keV is about 50% higher for the 'thick' sample from combined scattering, instead of being lower, as might have been expected from the preferential absorption of lower energy photons indicated by the relatively lower intensity of the Compton peak at 65 keV. The explanation for the higher intensity is that the probability for multiple scattering, to give a background contribution in the region between the incoherent and coherent scatter peaks, increases faster with sample thickness than the probability for single scattering represented by the coherent scatter peak.

Although the Compton profile is symmetrical, the intensity at energies below the Compton peak is generally higher than above it, as is evident in Figure 4.1. The additional intensity arises from incoherent scattering, mostly $>90^{o}$, in the source, scattered once more by the sample; source shield X-rays also are scattered by the sample.

4.3 Source-sample-detector (SSD) geometry

As shown later (chapters 6 and 7), in order to optimise the measurement of low gold concentrations in the reef, it is necessary to select both the gold X-ray peaks to be measured and the source so that the peak-to-background ratio is

maximized and the total background itself minimized. Because the background varies with the source-sample-detector geometry, some consideration must be given to the optimum geometry.

For a co-planar source and detector, increasing the SSD angle lowers the energy of the Compton peak thus reducing the background intensity at higher energies while increasing the intensity below it, and vice versa.

For Co-57 and higher energy sources, scattering angles considerably less than 180^{o} would appear to be preferable while for Cd-109 and lower energy sources angles closer to 180^{o} are more favourable.

Limiting the scattering angle to less than 180^{o} implies that the sample should be small relative to the radiation path lengths, defined by the collimation of the source and/or the detector. This is a rather inefficient measuring geometry. Without collimation, a massive sample would subtend between source and detector a range of angles from a minimum all the way up to 180^{o} and decreasing the minimum angle would, therefore, have little effect in reducing the background intensity at energies below the Compton peak; the reduction would be greater above the Compton peak when increasing the angle toward 180^{o}.

Gold determination in situ requires the measurement of rough-surfaced samples* where the distances of samples from

---

* A rough surface may be defined as one where, over the sample area, the root mean square deviation from a flat plane is of the same order of magnitude as the radiation path lengths.

the source and detector cannot be accurately controlled. The minimum scatter angle may thus fluctuate causing an energy shift of the Compton profile as well as changes in the shape of the background from multiple scattering. The variation in the shape of the background contributes a variance to the measurement of fluorescent gold peaks. The closer the minimum scattering angle is to 180^{o} the smaller will be its fluctuation for a given change in sample distance; the finite dimensions of detector and source preclude a scattering angle equal to 180^{o}.

For Cd-109 a number of SSD configurations were tested. In the earliest experiments only a 3mCi Cd-109 source was available and a high geometrical efficiency was sought by placing the source directly on the rock with the detector a few cm behind the source shield. This gave a relatively lower peak-to-background ratio for gold Kβ' peaks than was observed for the gold Kα peaks excited by Co-57. The source in contact with the sample allowed radiation emerging sideways (in a sligthly forward direction) to be scattered by the sample through as low as 90^{o} towards the detector, thus greatly increasing the background under the gold Kβ' peaks relative to that from a larger minimum scatter angle.

Subsequent measurements with the Cd-109 source placed close to the detector, and away from the sample, to increase the minimum scatter angle improved the gold peak-to-background ratio for Cd-109 so that it exceeded the ratio for Co-57.

In Figure 4.5 the Kβ spectral regions of a gold ore sample, of homogeneous concentration, are shown for central

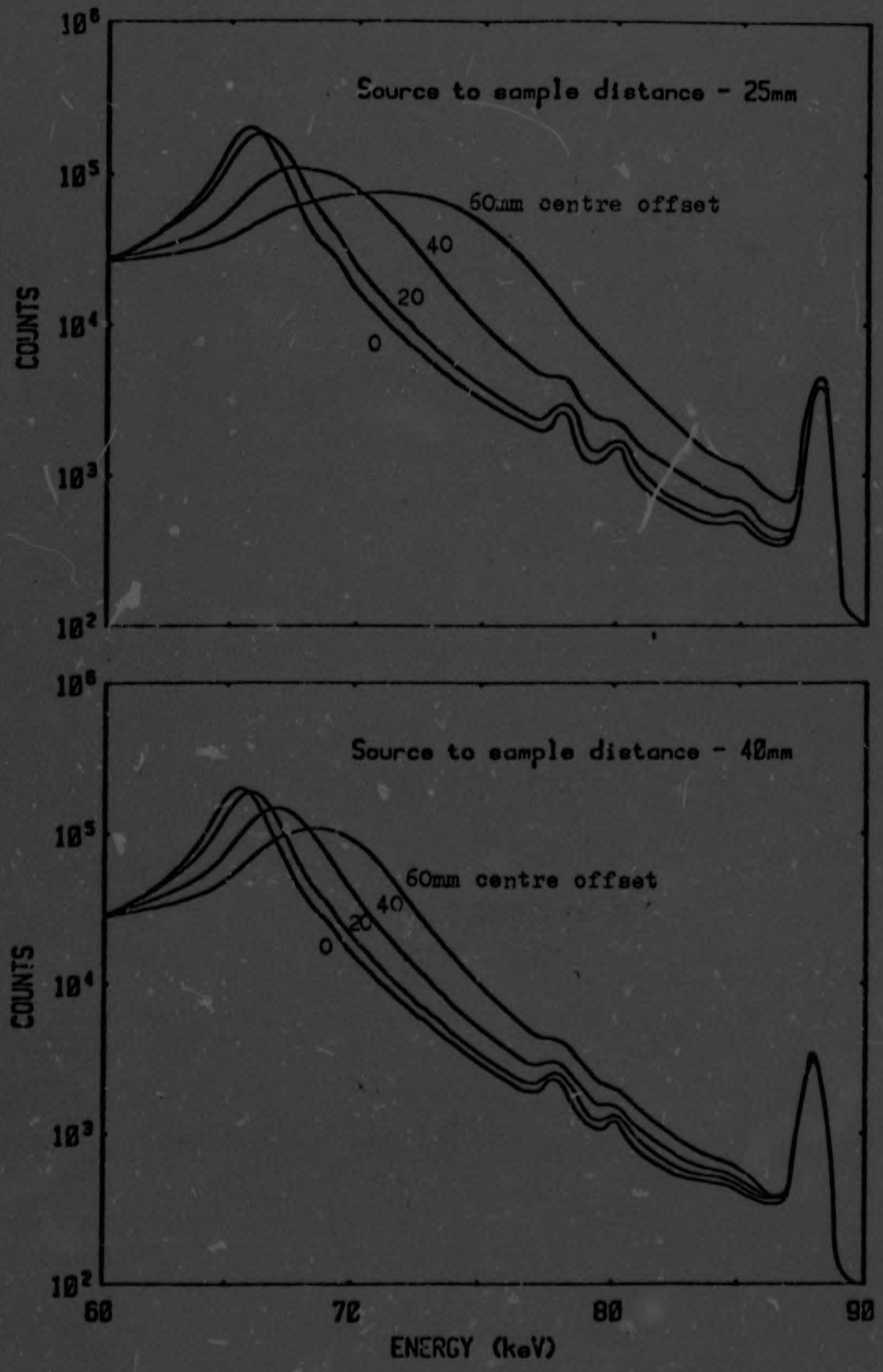


Fig. 4.5 Backscatter spectra from large sample of standard ore for different measuring geometries

and peripheral-source geometries. A 1,5mm diameter Cd-109 source was placed 3mm in front of and from 0mm to 60mm from the axis of a 16mm diameter x 10mm deep Ge detector; the surface of the standard ore sample was at distances of 25mm and 40mm from the detector, and source shield collimation was 120° towards the sample. Annular sources are often used for peripheral-source geometries but a set of point sources at the annulus radius gives the same results.

The spectra in Figure 4.5 were normalized to the Au $K\beta_1'$ peak intensity. A change in the slope of the background in the gold Kβ region may be observed. The highest peak-to-background ratio was obtained for the central source geometry.

In Figure 4.6 the relative increase of the backscatter

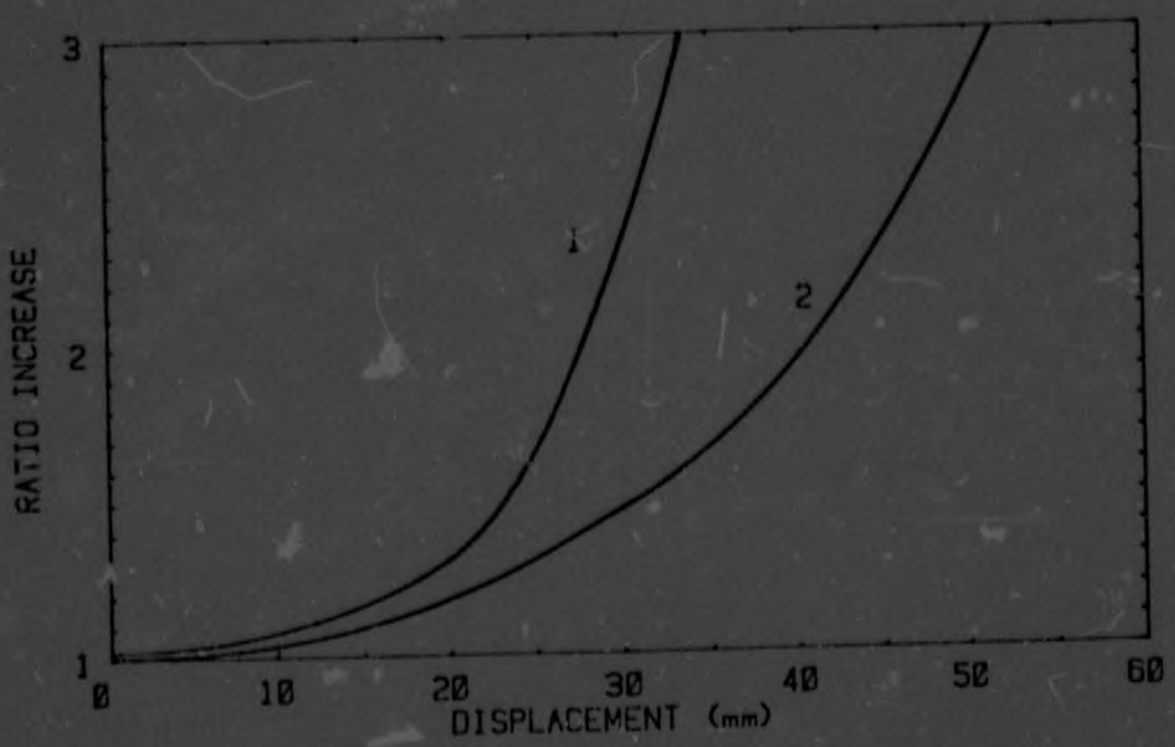


Fig. 4.6 Increase in backscatter intensity at 80keV from peripheral sources relative to that from a central source. Probe-to-sample distance: (1)-25mm, (2)-40mm

intensity at 78 keV (Au $K\beta_1'$) is shown relative to that from a central source geometry as a Cd-109 source is moved away form the detector axis. It will be shown in chapters 6 and 7 that, for a fixed peak intensity the measuring time required to attain the same precision of estimation for the peak-to-background ratio is directly proportional to the background intensity in the peak region, other conditions being equal.

For small displacements from the axis of the detector, shadowing from the source decreases the measuring efficiency. A tiny Cd-109 source and shield of 5,5mm outside diameter was developed, so that this shadowing amounted to 12%. Consequently a peripheral Cd-109 source would have to be less than 18mm from the detector axis to show a better performance than a central source of the same strength. Peripheral sources this close to the detector axis hardly offer any manufacturing advantage over a central source system. Moreover, the system for gold determination is limited by the electronic count-rate-handling capability of the measuring system, so that a central source of higher intensity can be employed to compensate for its shadowing effect.

In the second prototype of the portable gold analyser, in an attempt to produce a reliable source shutter, a peripheral source geometry was designed with three sources mounted at 26mm from the detector axis. When the full implication of the increase in measuring time with reduction in the minimum scattering angle was realised the design reverted to a central source geometry for the third prototype.

5 DETECTION OF FLUORESCENT SPECTRA

For rapid determination of gold the photon flux in the gold K X-ray region that emerges from the sample must be detected efficiently and with high energy resolution. The detector parameters which affect efficiency and resolution are evaluated below. In chapter 9 a balance is struck between high efficiency and high resolution, which leads to an optimum measuring time for the determination of gold.

5.1 Geometrical detection efficiency

A few cm away from a large rock sample irradiated by an uncollimated point source, located a similar distance away, the flux spreads over many tens of square centimetres and encompasses directions in a solid angle somewhat less than 2π steradians. With increasing detector area the efficiency increases as more of the flux is detected. However, only the return flux near the source has been scattered through a large angle, which is necessary to give a spectrum of the desired low background. An uncollimated detector of a few cubic centimetres volume located behind the source, should thus have an optimised geometrical efficiency together with the large angle scattering desired.

Detectors commercially available for X- and low energy gamma ray measurement are gas proportional tubes, sodium iodide scintillators and cryogenically cooled silicon and germanium semiconductors.

5.1.1 Detector thickness

For uncollimated measurement the linear absorption coefficient of the detector should be high enough to detect most of the gold K X-rays within a volume close to the source, i.e. within a detector thickness not much greater than its radius. The intensity of 80 keV photons is reduced by half every 310mm, 0,6mm, 13,6mm and 1,37mm in Xe(gas), NaI, Si and Ge respectively, showing that the absorption coefficients of proportional tubes and silicon detectors are too low for this application.

With Cd-109 excitation most of the backscattered radiation has lower energy than the gold Kβ lines. It is thus desirable to use a detector thickness where the gold Kβ lines are detected at close to 100% quantum efficiency since the lower energy radiation is detected with higher efficiency. On the other hand, if Co-57 (122 keV) or Te-123m (159 keV) excitation were to be used a thinner detector having a lower efficiency for this higher energy radiation would discriminate against the unwanted radiation, i.e. the detector filters the desired X-rays.

With Cd-109 excitation and Ge detectors the linear detection efficiency for 80 keV and 65 keV photons and their ratio is shown in Figure 5.1. There is little improvement in the 80 keV/65 keV efficiency ratio for detectors thicker than three to four millimetres. However, the electronic noise resolution of the detector system improves with the lower capacitance of thicker detectors. A limitation on increasing the thickness is the maximum

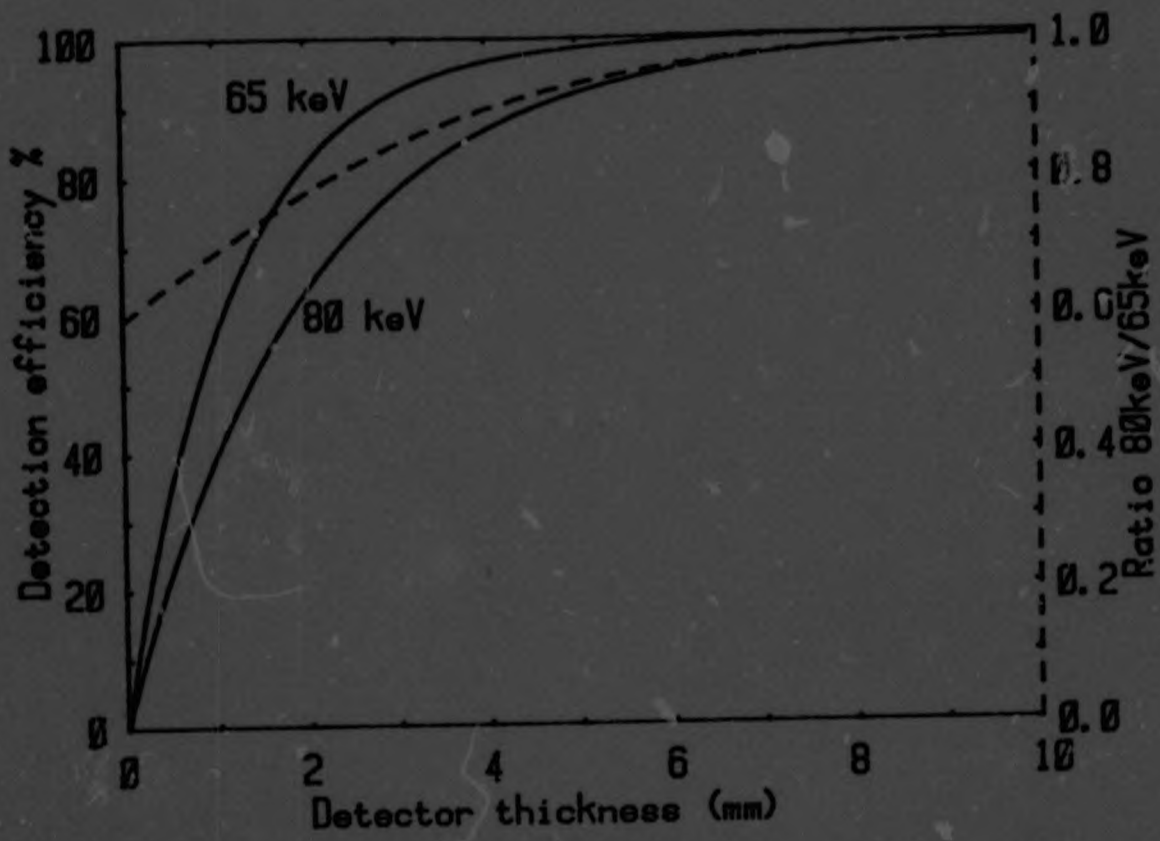


Fig. 5.1 Linear detection efficiencies and their ratio vs. Ge detector thickness

desirable charge collection time, which amounts to 10ns/mm in the detector, since this proportionally affects the pulse-pair-resolution time for amplifier pileup rejection.

From these considerations, a Ge detector thickness of 7mm appears near optimum.

5.2 Energy resolution

In the X-ray region below 30 keV excellent line resolution can be attained with crystal diffractometers, i.e. wavelength dispersive systems. Their geometrical efficiency is, however, extremely low because only radiation from the sample collimated to fractional millisteradians is measured. The low geometrical efficiency requires a complementary high flux which is in practice available only

from X-ray tubes. In the gold K X-ray energy region, the crystals of wavelength dispersive systems also have a low diffraction efficiency and in fact have a poorer resolution than germanium detectors.

Sodium iodide (thallium activated) would be the most convenient type of photon detector because it requires no cooling and is highly efficient, but its energy resolution is rather poor in the X-ray region and additional energy discrimination would be required such as crystal diffraction or a pair of balanced filters which, by selective absorption, allow the determination of single elements in paired measurements.

Semiconductor detectors have inherently a high energy resolution for X-rays and may be used without additional energy discrimination. An inconvenience, particularly for portable applications, is that this resolution is realized only at cryogenic temperatures, conventionally at 77°K (liquid nitrogen). The development in recent years of hyperpure germanium has, however, greatly reduced the cooling problem which prior to this meant lifetime cooling of the detector to prevent undrifting of compensating lithium ions. Warmup of these detectors between daily operation no longer has a deleterious effect on the resolution.

The energy window of a pair of platinum/iridium balanced filters (whose thicknesses are balanced to exhibit the same absorption characteristics outside their energy window) for the measurement of the gold $K\beta_1$ lines is 2,28 keV, while the resolution of a thin NaI scintillator crystal for associated

background measurement is about 11 keV FWHM. These parameters may be compared to the 0,6 keV FWHM resolution of a germanium detector, which permits simultaneous measurement of peak and background and thus enables gold to be determined with a germanium detector at least ten times, and probably closer to a hundred times faster, than with balanced filters and a thin NaI crystal.

5.2.1 Resolution of germanium detectors

The energy resolution of a germanium detector is a function both of the photon energy and of the electronic noise of the detector system.

The FWHM energy resolution of the system is given by (Woldseth, 1967)

$$\Gamma = \sqrt{(5{,}55\ F\varepsilon E + \Gamma_n^2)} \qquad 5.1$$

where

F = Fano factor $\sim$ 0,125 for Ge

ε = energy per hole electron pair $\sim$ 2.93eV in Ge

E = photon energy (in eV)

Γ_n = FWHM system noise resolution

The constant 5,55... converts squared units of FWHM to standard deviations.

In what follows, the approximate resolution of a germanium detector is taken at 80 keV (the energy of the gold $K\beta'_2$ lines) and a preliminary evaluation of the noise resolution is made. Further calculations of the noise resolution are given in chapter 9.

The inherent resolution for germanium at 80 keV, i.e. if there were no electronic noise (Γ_n=0), is 406eV (i.e. 5,55x0,125x2,98x80000eV). Cooled field effect transistors

and pulsed-optical-feedback circuits are commercially available with an electronic noise performance which matches the still smaller inherent resolution at lower photon energies. At 80 keV, however, resistive feedback provides adequately low noise performance, and at the same time permits operation at higher count-rates than does pulsed-optical feedback.

The noise resolution Γ_n depends on the amplifier time constant TC, the capacitance of the detector system and on the baseline instability of the amplifier at high count rates.

Integration over time of the equivalent series and parallel noise gives respectively an inverse and direct square root dependence on the system time constant TC for the two noise components -

$$\Gamma_n(\text{series}) \propto 1/\sqrt{TC}$$

and $\Gamma_n(\text{parallel}) \propto \sqrt{TC}$

while $$\Gamma_n^2 = \Gamma_n^2(\text{series}) + \Gamma_n^2(\text{parallel}) \qquad 5.2$$

This is indicated by the dashed lines in Figure 5.2. For time constants TC shorter than 2μs the total noise resolution is predominantly caused by serial noise and the parallel noise contribution may be disregarded. In this figure the resolution of a typical Ge detector 200mm^{2}x7mm thick measured at several time constants TC is shown as well as the noise resolution of the system with a pulser.

The noise resolution is proportional to the capacitance of the detector system. For a planar detector the capacitance is given by the permittivity x area/thickness. Thus a 7mm thick Ge detector has a capacitance of about

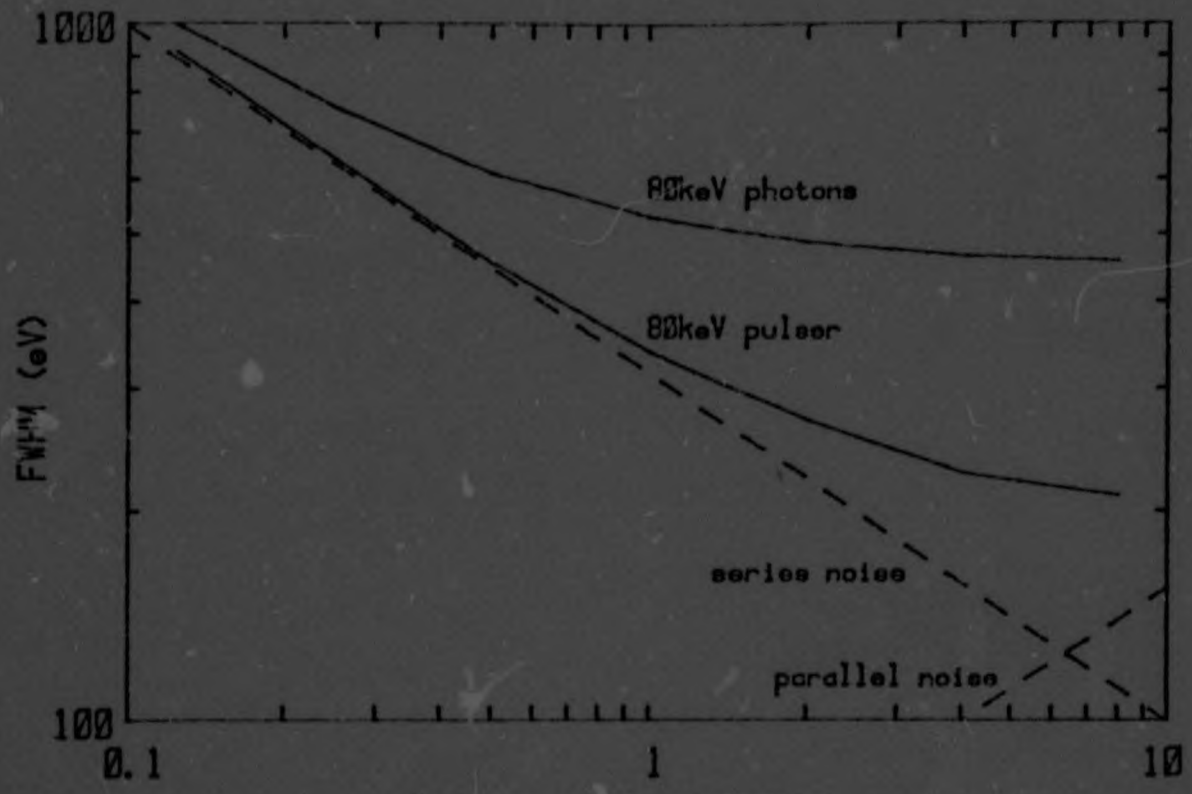


Fig. 5.2 Energy resolution of a 200mm x 7mm Ge detector

22,5pF/mm^2 and the stray capacitance in a typical detector system is about 5pF. This gives the noise resolution as -

$$A\Gamma_n \sim {}_{100}\Gamma_n(0,0225A + 5)(2,25 + 5) = (0,003A + 0,7)\,{}_{100}\Gamma_n \quad 5.3$$

where A = area of detector in mm^2; thickness 7mm

${}_{100}\Gamma_n$ = noise resolution of 100mm^2 detector

Combining this with ${}_{200}\Gamma_n \sim 310/\sqrt{TC}$ eV the approximate noise resolution at time constants shorter than 2μs is given by

$$A\Gamma_n \sim (0,003A + 0,7)310/1,3\sqrt{TC}\ \text{eV}$$

$$\sim (0,73A + 163)/\sqrt{TC}\ \text{eV} \quad 5.4$$

and with equation 5.1, the system energy resolution at 80 keV is

$$\Gamma \sim \sqrt{[406^2 + (0,73A + 163)^2/TC]}\ \text{eV} \quad 5.5$$

Degradation of the resolution and peak shift at high count rates is largely caused by instability of the

amplifier baseline which is additive to the amplifier peak height. With good baseline restoration, amplifier duty cycles as high as 95% can be tolerated, whereas with poorer restoration, instability may be noticed at duty cycles of 40% or even lower. In the gold detector duty cycles are maintained below 30% so as to keep the signal processing efficiency high. Degradation of the resolution and peak position with highly varying count rates, as encountered in scanning rough rock faces, should, therefore, be low.

It has been shown above that, for gold determination with Cd-109 excitation, the detection efficiency of a germanium detector is closely proportional to its area and the energy resolution is a function of the area and system time constant given by equation 5.5. These relationships will be used in chapter 9 to derive the optimum detector size and system time constant for gold determination.

6 FUNDAMENTALS IN SPECTRUM EVALUATION

In previous chapters, optimisation of the throughput of a detector amplifier sub-system was discussed. All too often a great deal of attention is paid to the throughput of this sub system while the evaluation of the output spectrum is treated rather poorly, resulting in reduced total system performance. In this chapter, handling of the amplifier output in the portable instrument is discussed. Although highly efficient spectral evaluation is desired, at the present time instrument simplicity may dictate a slightly reduced efficiency. Advances in technology may in the future lead to more complex portable instruments less restricted in the evaluation of the amplifier output. It is shown, however, that the benefits to be gained from additional complexity are likely to be small.

The output from the amplifier is a spectrum of pulse heights. A finely differentiated pulse height or energy spectrum can be obtained by employing an analog-to-digital converter - multichannel system. In this type of system the height of a pulse is analysed by small incremental steps. Alternatively, selected parts of the spectrum can be coarsely differentiated into a few channels by means of separate pulse height discriminators in a set of single channel systems.

In a finely differentiating system, the processing time

or deadtime of the pulse-height-analysis sub-system can sometimes adversely affect the total system output rate. For gold determination, the backscatter spectrum from a rock face would, however, require fine differentiation over only a limited region. This region has a very low count rate relative to that of the total spectrum and fine differentiation in this case need not reduce the useful output rate by more than one percent at the highest practical rates.

The spectral features of importance here are peaks and the background under and adjacent to the peaks. The instrumental response to a monoenergetic line may be considered as purely Gaussian. Although intense single peaks may also show non-Gaussian tails, these are usually small and need not concern us here. The background in the peak region can be considered as a smooth function with no peak structure.

The extent of the spectral region suitable for the evaluation of a peak and its background is normally limited by neighbouring peaks and by the correlation of the background away from the peak to that under the peak.
In the following sections the evaluation of a single peak and its background will be treated analytically. In the following chapter the theoretical results will then be applied to the gold region of the backscatter spectrum.

6.1 Gaussian peak on a constant background

A single Gaussian peak on a constant background will be considered here. Other smooth background functions can readily be related to this simple constant function. For

this case, spectrum evaluation involves the separate determination of peak and background intensities from two or more measured intensity values of various parts of the spectrum. At a given background rate, the standardized variances obtained are directly proportional to the measurement times which would be required to obtain the same measurement precision by the different evaluation schemes. These variances thus form a basis for the objective optimization of the spectrum evaluation.

6.2 Generalized evaluation

For comparison of different evaluation methods a normalized co-ordinate system, shown in Figure 6.1, is chosen, where the peak resolution is given by the Gaussian parameter $\sigma=1$. The total peak intensity, when integrated from $-\infty$ to $+\infty$, is defined as P units, while the background has an intensity B per unit peak standard deviation. The peak to background ratio R can then be defined as $R = P/B$.

In this normalized co-ordinate system the peak height is $P/\sqrt{(2\pi)}$ and the FWHM resolution is $\sqrt{(8\ell n2)} = 2,35..$. When the normalized R needs to be converted to peak-height ratio, R should be multiplied by $1/\sqrt{(2\pi)} = 0,398..$, while for conversion to FWHM peak area per FWHM background area, R should be multiplied by $\sqrt{(2/\pi)}\int_0^{\sqrt{(2\ell n2)}} \exp(-t^2/2)\,dt = 0,429..$.

Measurements in a spectral region can be performed in a number i of independent measuring channels, each bounded by lower and upper discriminators at energies $_\ell t$ and $_u t$ respectively, as illustrated in Figure 6.2. For fine differentiation a large number of contiguous channels

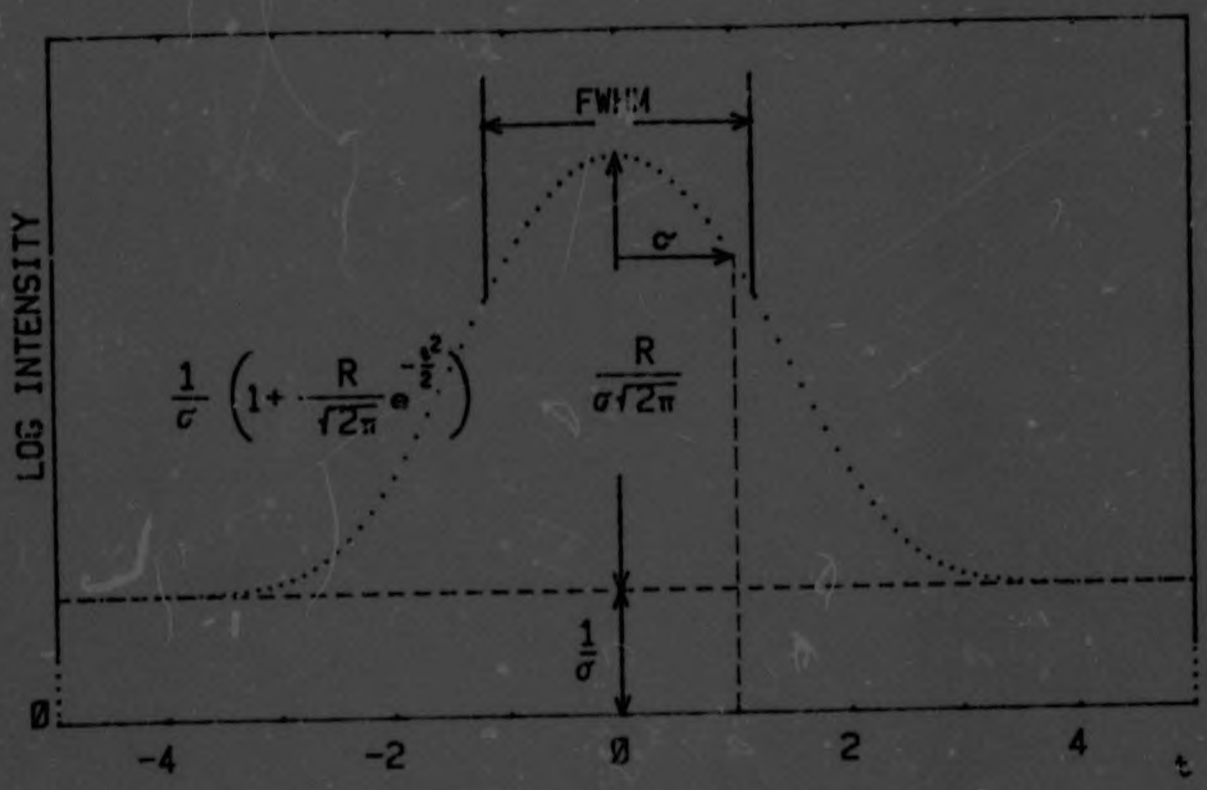


Fig. 6.1 Normalized Gaussian peak and background

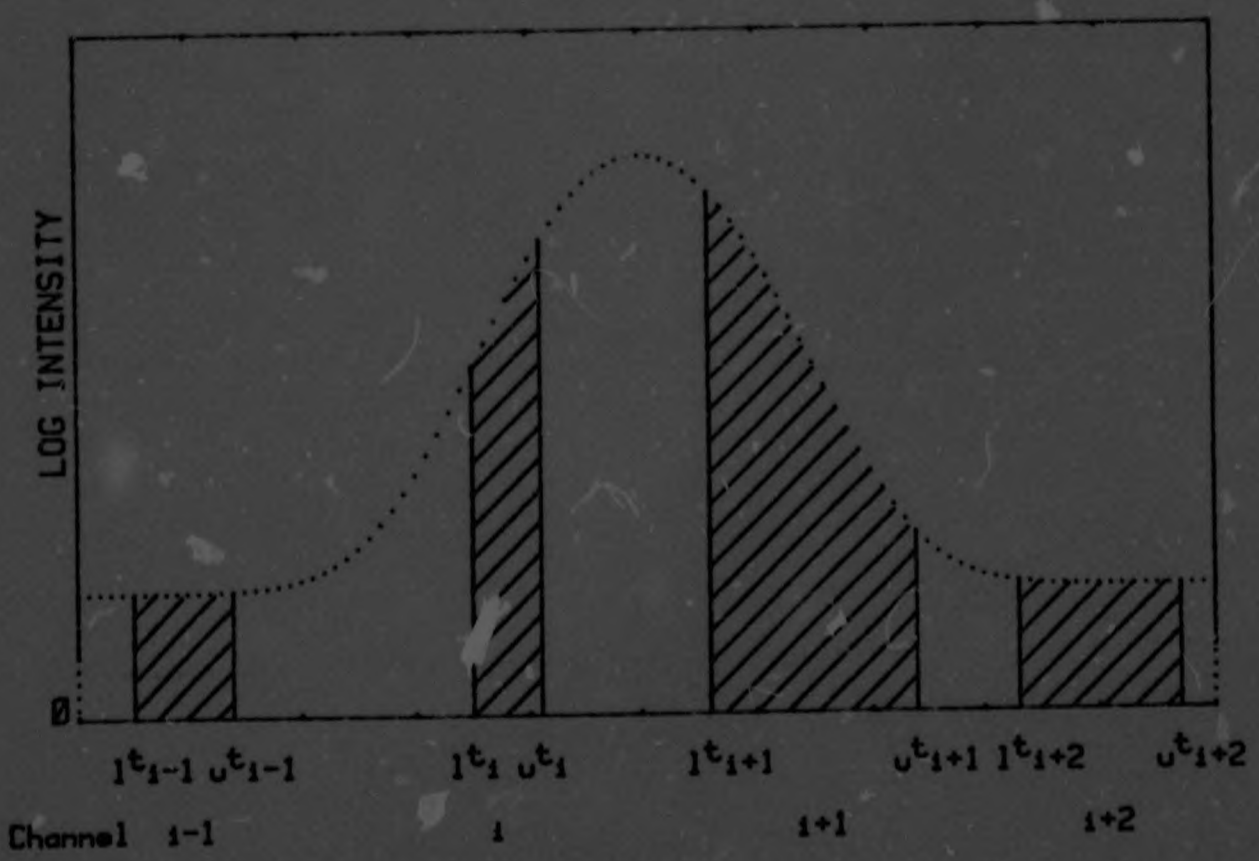


Fig. 6.2 General peak and background measurement

$({}_u t_i = {}_\ell t_{i+1})$ of equal energy increments $({}_u t_i - {}_\ell t_i = {}_u t_{i+1} - {}_\ell t_{i+1})$ are employed so that there are several channels per peak standard deviation. In coarse differentiation a minimum number of two channels, of non-equal energy increments, or spaced asymmetrically about the peak, is required.

At a true peak and background intensity $\hat{P}$ and $\hat{B}$ the expected intensity in each measuring channel is given by -

$$\begin{aligned} Y_i &= \hat{B}\,({}_u t_i - {}_\ell t_i) + \hat{P}\,({}_{\ell t_i}\textstyle\int^{{}_u t_i} \mathrm{Exp}(-t^2/2)\,dt/\sqrt{(2\pi)} \\ &= \hat{B}\,t_i + \hat{P}\,G_i \\ &= \hat{B}\,(t_i + \hat{R}\,G_i) \end{aligned}$$

The intensities are Poisson variables, and the expected mean and variance thus have the same value -

$$\begin{aligned} V[Y_i] &= \hat{Y}_i \\ &= \hat{B}\,t_i + \hat{P}\,G_i \\ &= V[Bt_i] + V[PG_i] \end{aligned}$$

A solution for P and B can be obtained from measured intensities by the following weighted least squares calculation

$$\begin{vmatrix} P \\ G \end{vmatrix} = \begin{vmatrix} \sum_i G_i^2 W_i & \sum_i t_i G_i W_i \\ \sum_i t_i G_i W_i & \sum_i t_i^2 W_i \end{vmatrix}^{-1} \begin{vmatrix} \sum_i Y_i G_i W_i \\ \sum_i Y_i t_i W_i \end{vmatrix}$$

$$= \frac{1}{D} \begin{vmatrix} \sum_i t_i^2 W_i & -\sum_i t_i G_i W_i \\ -\sum_i t_i G_i W_i & \sum_i G_i^2 W_i \end{vmatrix} \begin{vmatrix} \sum_i Y_i G_i W_i \\ \sum_i Y_i t_i W_i \end{vmatrix}$$

where the determinant is -

$$D = \frac{1}{2} \sum_i \sum_j (t_i G_j - t_j G_i)^2 W_i W_j$$

The solution of maximum likelihood would be obtained with weighting factors W_i equal to the reciprocal of the true variance of Y_i i.e. for

$$W_i = 1/V[Y_i]$$

$$= 1/\hat{Y}_i$$

In a measuring situation the true means and variances are unknown. If, however, the measured intensities are high enough then they can be taken as a good approximation for the true values -

$$Y_i \xrightarrow{i >> 1} \hat{Y}_i$$

When the measured intensities Y_i are small, the least squares calculation can be performed without the weighting factors W_i - usually with little deterioration in accuracy of the results. The first calculation can be followed by one or two iterative calculations using improved weighting factors.

In two-channel analysis the same means are obtained with or without weighting factors but the variance is affected by the weighting factors.

6.3 Variance of the peak to background ratio

In the present analytical evaluation with a priori knowledge of the P and B, the true values of $1/\hat{Y}_i$, even at low intensities, are available as weighting factors for the variance analysis of expected P and B.

The variance of P and B are given by the diagonal elements of the square covariance matrix -

$$V[P] = \frac{1}{D} \sum_i t_i^2/\hat{Y}_i$$

$$V[B] = \frac{1}{D} \sum_i G_i^2/\hat{Y}_i$$

The variance of the peak-to-background ratio, derived by the delta method (Hawkins, 1975), involves all the elements -

$$V[P/B] = \frac{1}{D}\left(\sum_i t_i^2/\hat{Y}_i + 2R \sum_i t_i G_i/\hat{Y}_i + R^2 \sum_i G_i^2/\hat{Y}_i \right)$$

$$= \frac{\hat{B} \sum_i (t_i + \hat{R} G_i)}{\frac{1}{2} \sum\sum_{ij} \frac{(t_i G_j - t_j G_i)^2}{(t_i + RG_i)(t_j + RG_j)}}$$

The last equation, in various forms, was applied to the differential multichannel and to the three single channel-schemes for spectrum-evaluation shown in Figure 6.3. The background intensity was standardized to a single (Poisson) count per peak standard deviation, i.e. B=1, to allow comparison of variances. Only the region t>=0 was considered because peak and background are symmetrical about t=0. This one-sided analysis facilitates adaptation of the evaluation scheme to real situations where the spectrum on one side of a peak often differs from that on the other side.

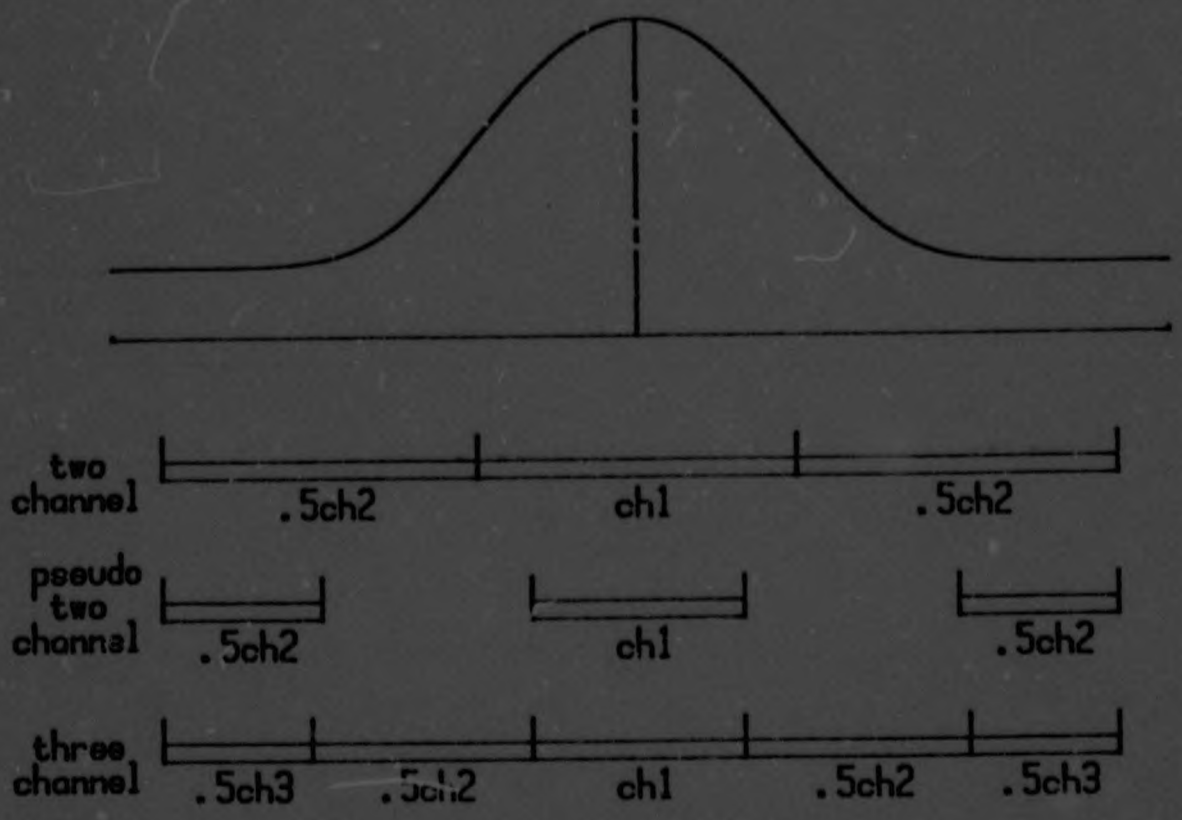


Fig. 6.3 Single channel schemes for peak evaluation

Variances were computed for a series of peak to background ratios R from 1000 to 0,01 and R=0, and for a range of maximum available background regions, t_{max} from infinity to 1σ, where the highest discriminator would be positioned.

In Figure 6.4 the standardized background multichannel (superscript m) variance ${}^{m}_{R}V_{t_{max}}$ of the peak-to--background ratio with an unlimited background region, i.e. $t_{max} \longrightarrow \infty$, is shown for the above series of peak-to-background ratios. For R=0 we have ${}^{m}_{0}V_{\infty} = 4\sqrt{\pi} = 7,09$ and a logarithmic scale of ${}^{m}_{R}V_{\infty} / {}^{m}_{0}V_{\infty} - 1$ was chosen for clarity in presentation of the variance. In Figure 6.5 the standardized multichannel variance at limited background regions divided by those at unlimited background, from the previous figure, ${}^{m}_{R}V_{t_{max}} / {}^{m}_{R}V_{\infty}$ are given. The relative variances are plotted on a logarithmic scale of ${}^{m}_{R}V_{t_{max}} / {}^{m}_{R}V_{\infty} - 1$ while the maximum available background region is plotted on a log scale of $(t_{max} - 0,67\sigma)$, the constant 0,67 relating to the probability of 0,5, since $\sqrt{(2/\pi)}\int_{0}^{0,67} Exp(-t/2)dt = 0,5$. These curves illustrate the ultimate improvement factor possible in differential multichannel evaluation if an unlimited background region were available.

In single channel schemes the variance for a given R and t_{max} depends on the position(s) of the intermediate discriminator(s). The variance equations when partially differentiated with respect to the intermediate discriminator position(s) and equated to zero, lead to transcendental equations involving normal integrals. The minimum variances were, therefore, computed by successive

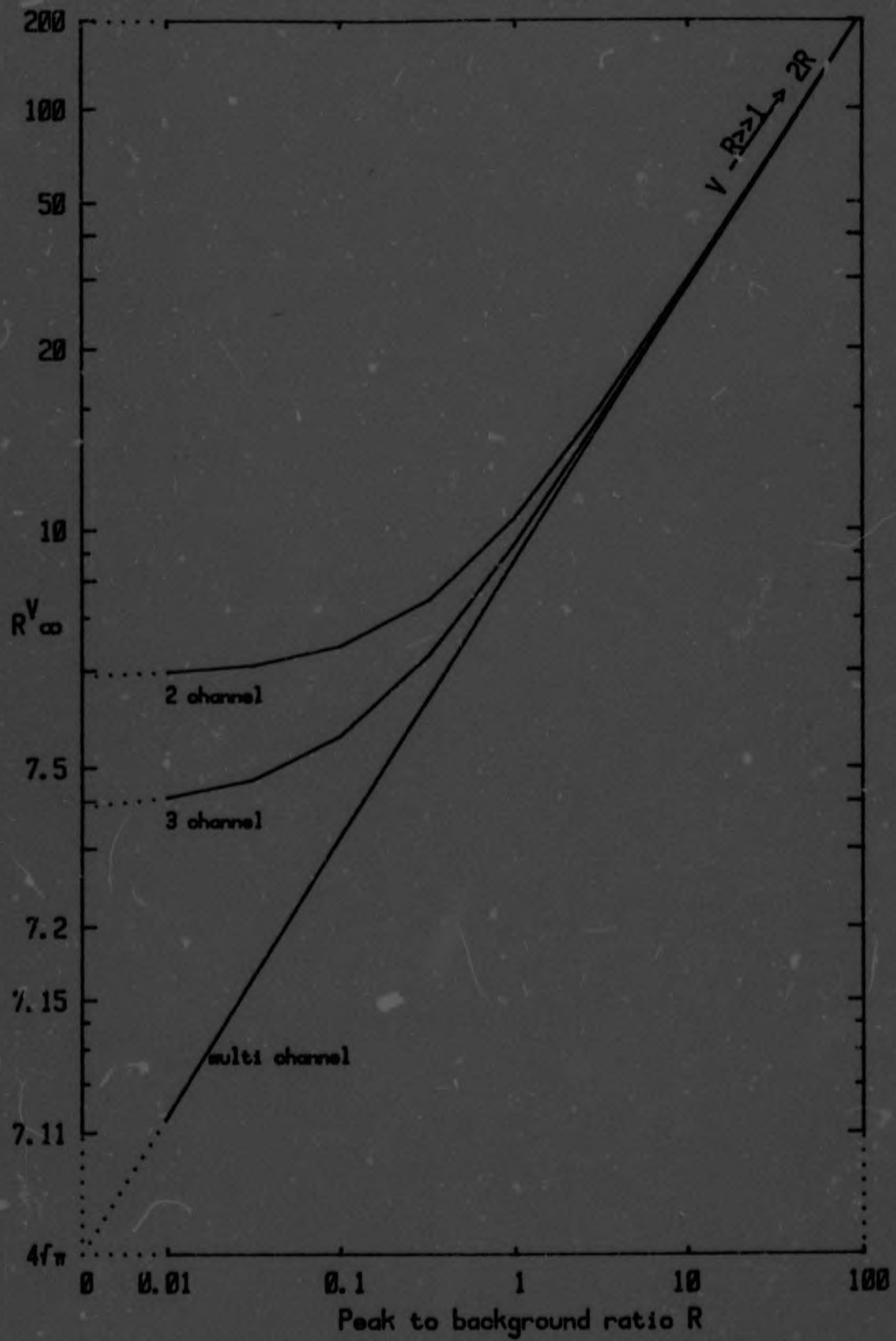


Fig. 6.4 Standardized background variances of R ; background region unlimited

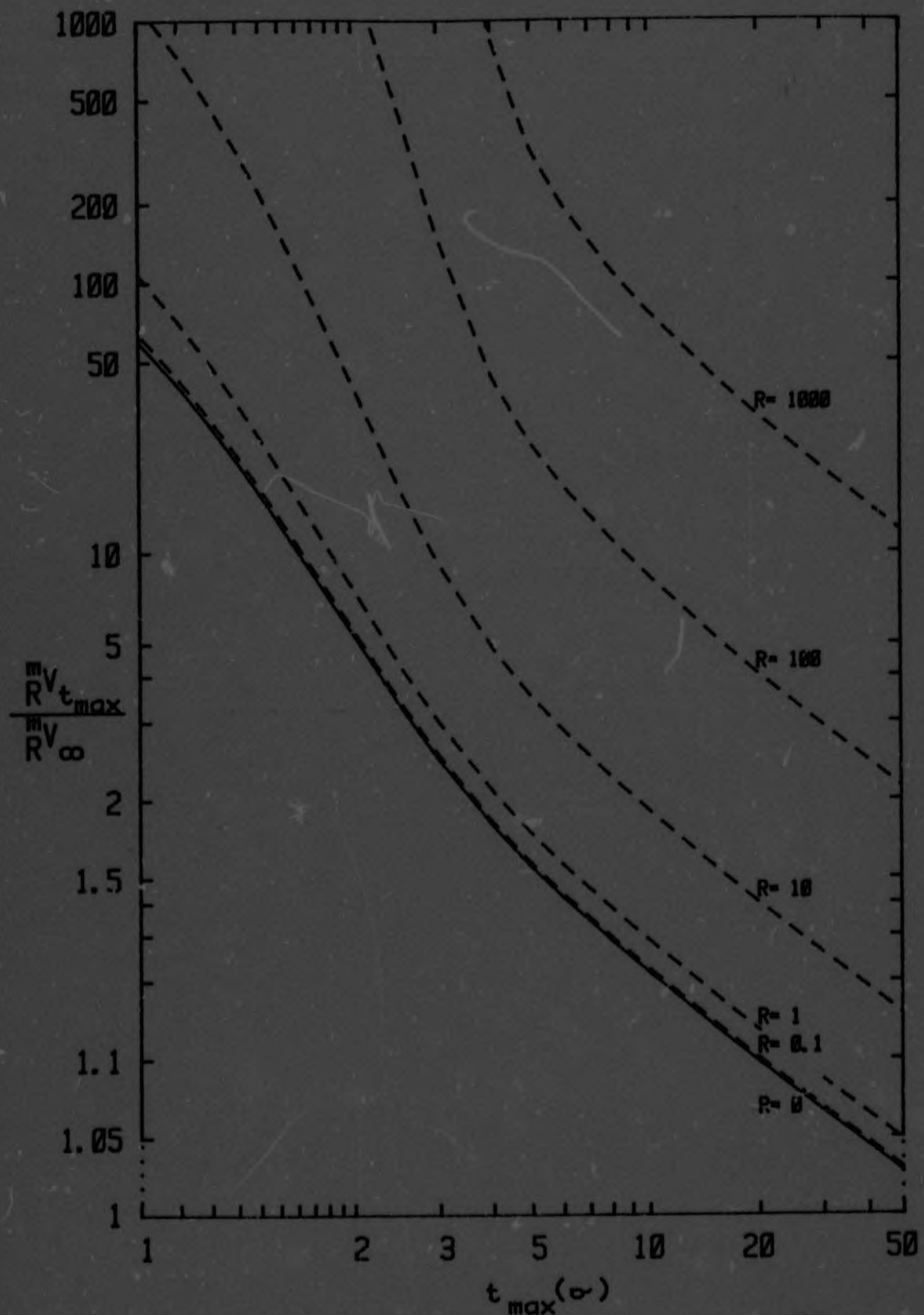


Fig. 6.5 Standardized multichannel variance ${}^{m}V_{t_{max}}$ relative to ${}^{m}V_{\infty}$

approximation of the intermediate discriminator position(s).

Single channel schemes for spectral peak-to-background ratio evaluation employ two or more counting channels. Usually an even number of pulse-height-discriminators is used. A discriminator at the peak centre serves no purpose. An odd number of discriminators would thus be unevenly distributed between the two sides of the peak. This special situation need not concern us here. Mention should, however, be made of the lowest scheme of two contiguous counting channels with 3 discriminators - this can be useful where the background is highly asymmetrical about the peak or where it is imperative to use the lowest posible number of discriminators.

With the same number of discriminators on both sides of the peak the corresponding spectral regions can be counted in the same counting channel. In this analysis only one side of the peak and background region was considered, with the same number of counting channels and half the number of discriminators as used in the whole region. Variances of the peak-to-background ratio were computed for the three single-channel schemes illustrated in Figure 6.3 -

a) ^{2}V for 2 discriminators on a side with two contiguous counting regions - this will be referred to as the 2 channel scheme;

b) ^{3}V for 3 discriminators with three contiguous counting regions - referred to as the 3 channel scheme, and

c) $^{3:2}V$ for 3 discriminators with two non-contiguous counting regions referred to as the pseudo 2 channel scheme; data between the two regions is discarded.

The attraction of using only two counting channels lies

approximation of the intermediate discriminator position(s).

Single channel schemes for spectral peak-to-background ratio evaluation employ two or more counting channels. Usually an even number of pulse-height-discriminators is used. A discriminator at the peak centre serves no purpose. An odd number of discriminators would th s be unevenly distributed between the two sides of the peak. This special situation need not concern us here. Mention should, however, be made of the lowest scheme of two contiguous counting channels with 3 discriminators - this can be useful where the background is highly asymmetrical about the peak or where it is imperative to use the lowest posible number of discriminators.

With the same number of discriminators on both sides of the peak the corresponding spectral regions can be counted in the same counting channel. In this analysis only one side of the peak and background region was considered, with the same number of counting channels and half the number of discriminators as used in the whole region. Variances of the peak-to-background ratio were computed for the three single-channel schemes illustrated in Figure 6.3 -

a) ^{2}V for 2 discriminators on a side with two contiguous counting regions - this will be referred to as the 2 channel scheme;

b) ^{3}V for 3 discriminators with three contiguous counting regions - referred to as the 3 channel scheme, and

c) $^{3:2}V$ for 3 discriminators with two non-contiguous counting regions referred to as the pseudo 2 channel scheme; data between the two regions is discarded.

The attraction of using only two counting channels lies

in the simplicity of calculating P and B by the linear algorithms -

$$\begin{vmatrix} P \\ B \end{vmatrix} = \frac{1}{D} \begin{vmatrix} t_2 & -t_1 \\ -G_2 & G_1 \end{vmatrix} \begin{vmatrix} Y_1 \\ Y_2 \end{vmatrix}$$

where $D = G_1 t_2 - G_2 t_1$

and $\frac{P}{B} = (t_2 Y_1/Y_2 - t_1)/(-G_2 Y_1/Y_2 + G_1)$

If a preset count is accumulated in channel 1 or 2 then P, B and P/B can be calculated from the count Y in channel 2 or 1 respectively by $A_1 Y + A_2$, where in the case of P and B the A's are constants and in the case of P/B the A's are functions of Y, but can usually be taken as constants for small values of P/B or over limited ranges of P/B.

When more than two counting channels are used then calculation of the algorithms becomes slightly more laborious and, as indicated in section 6.2, weighting factors $w_i = 1/V[Y_i]$ ought to be used.

In Figures 6.6a to 6.8a the standardized variances of the peak-to-background ratio in single channel analysis relative to those in multichannel analysis are shown. The corresponding positions of the intermediate discriminators, at which the minimum variance occurs, are shown in the (b) parts of the figures. The maximum available background region t_{max} is again plotted on a log scale of $(t_{max}-0,67\sigma)$.

The absolute values of the standardised variances can readily be obtained by multiplying the relative variances in these figures by the appropriate factors from Figures 6.4 and 6.5.

These variances have to be halved when combining the evaluation of both (symmetrical) sides of a peak and have to

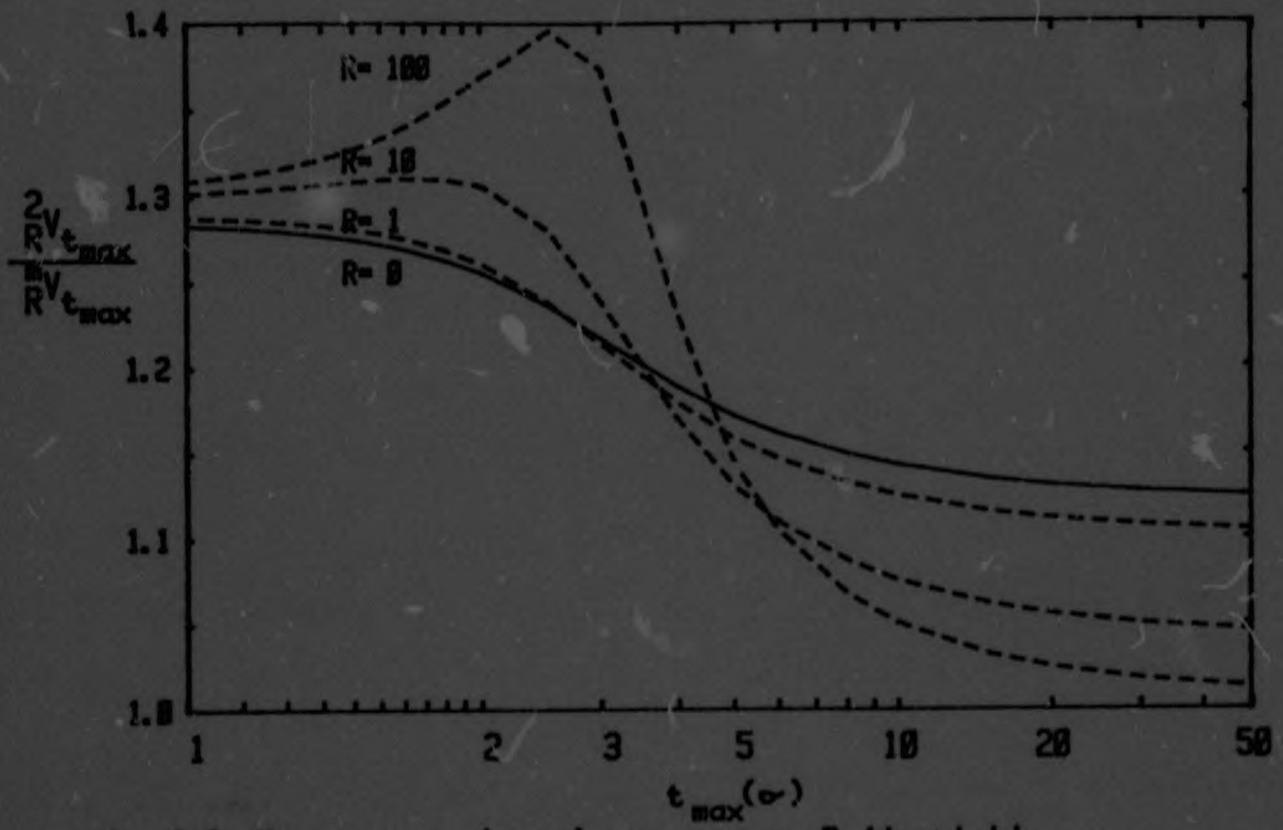


Fig. 6.6a Minimum two channel variance in R (divided by multichannel variance)

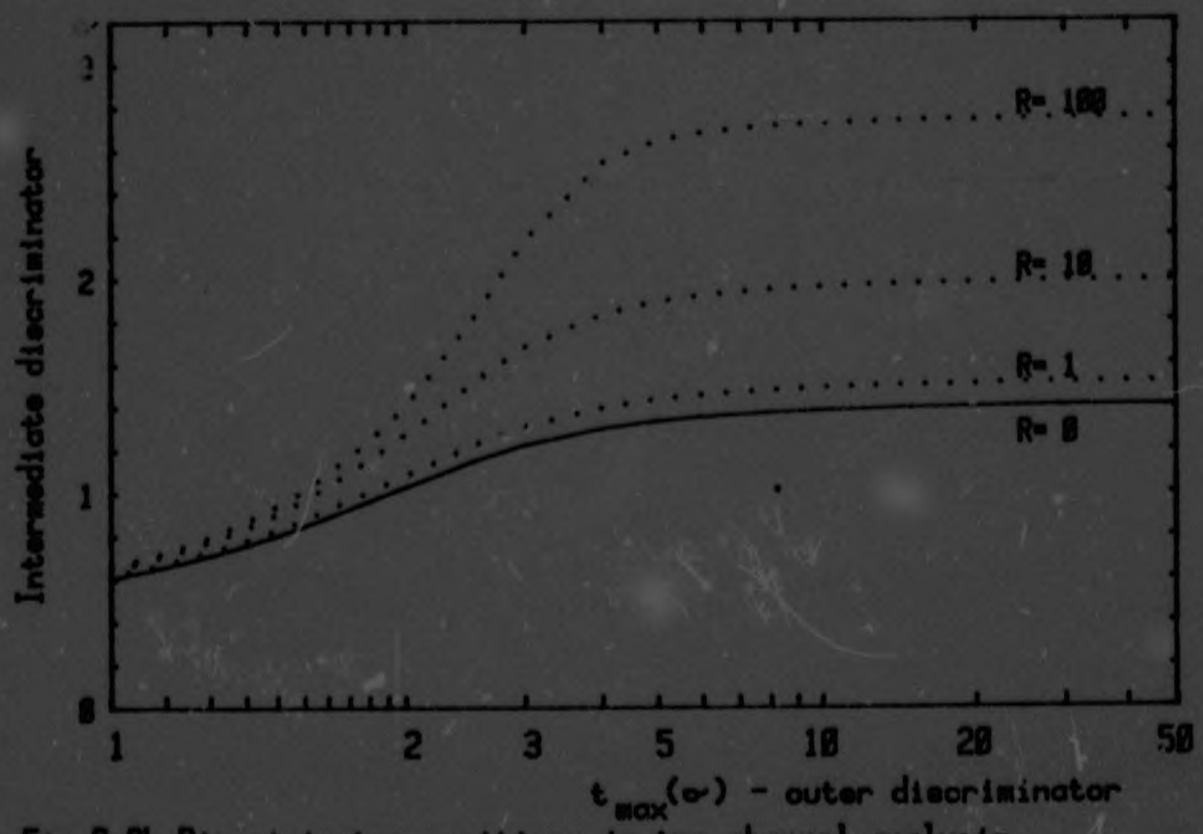


Fig. 6.6b Discriminator positions in two channel analysis for minimum variance in R

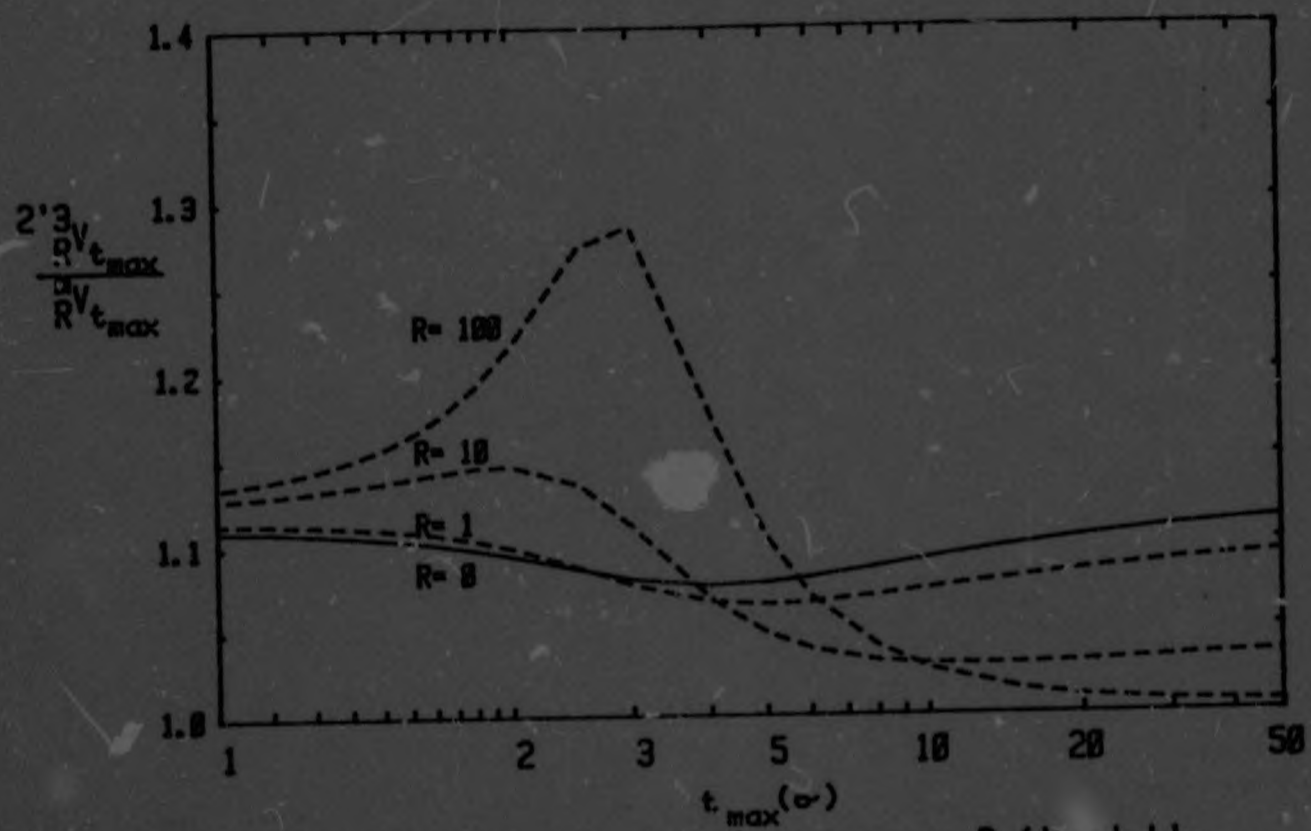


Fig. 6.7a Minimum pseudo two channel variance in R (divided by multichannel variance)

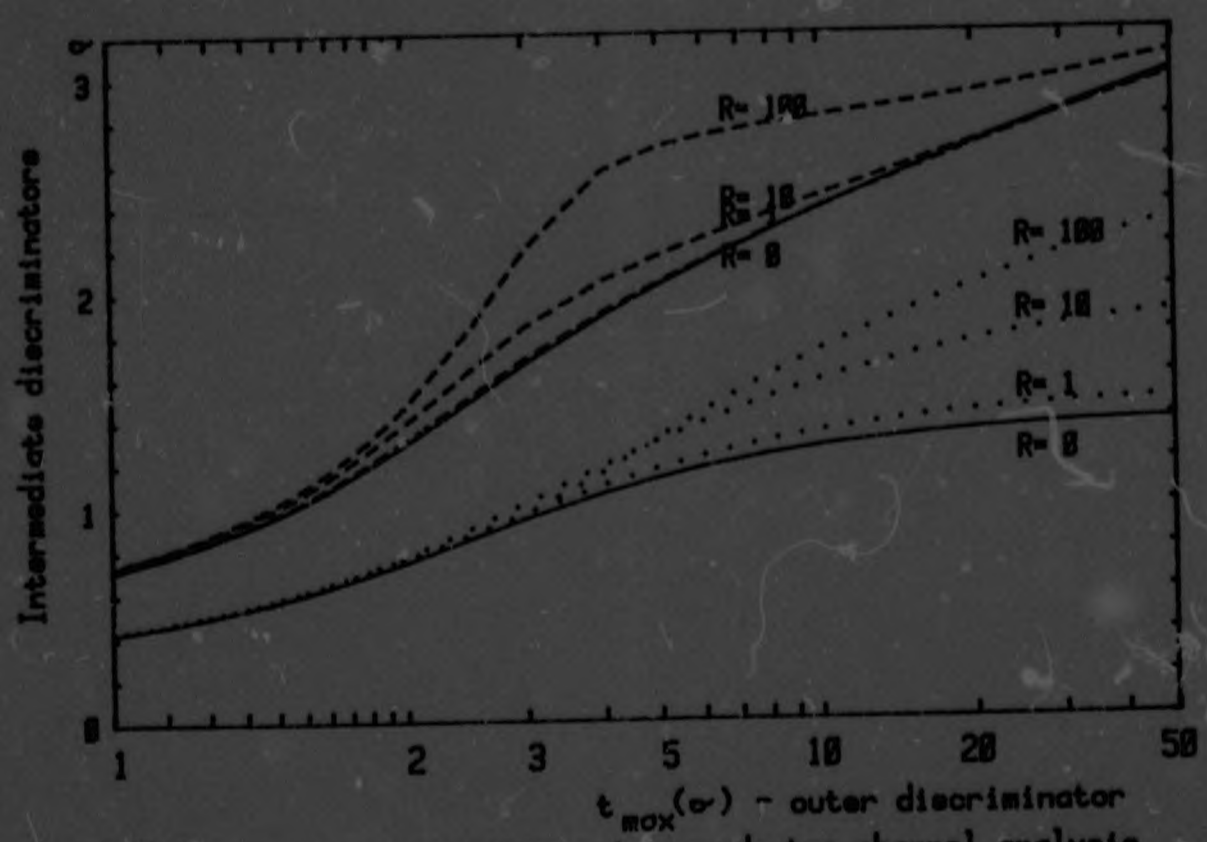


Fig. 6.7b Discriminator positions in pseudo two channel analysis for minimum variance in R

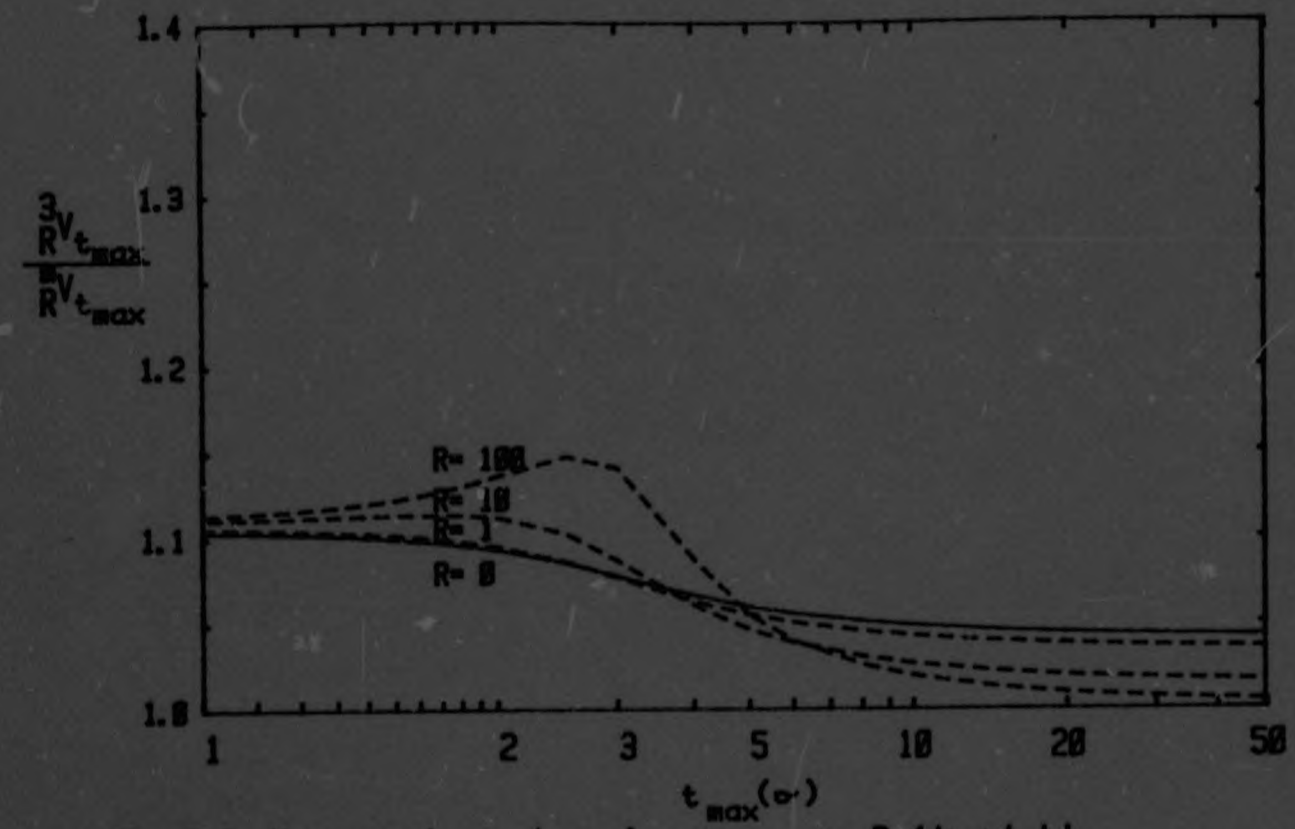


Fig. 6.8a Minimum three channel variance in R (divided by multichannel variance)

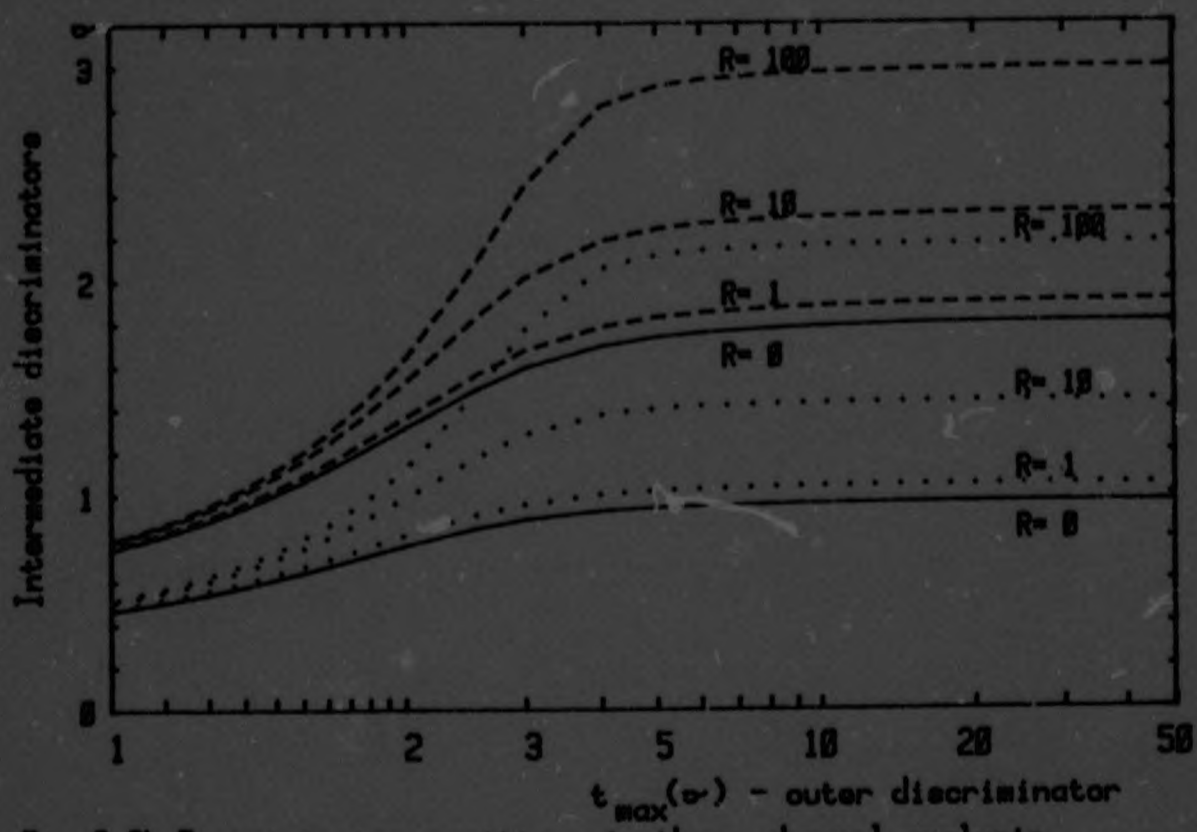


Fig. 6.8b Discriminator positions in three channel analysis for minimum variance in R

be divided by B for non-standardised background conditions. The relative presentation permits ready comparison of the different evaluation schemes.

6.4 Comparison of multichannel and few channel methods

The multichannel variances shown in Figure 6.4 may be considered as the inherent standardised variances of the peak-to-background ratios under standardised background conditions. It may be seen that when ^{m}R increases from 0 to 1 the variance increases by only 32% (from 7,09 to 9,4) because it is dominated by the standardised background, whereas at high ratios the increase is much greater as the inherent variance tends to the value 2R. At high ratios, the peak intensity on its own is usually more important than the peak-to-background ratio but at low ratios the opposite is often the case, as it is in the gold detection problem.

From Figure 6.5, it may be seen that, for ratios below R=1, little improvement in variance is to be gained by using background regions beyond $t_{max}^{0.10\sigma}$ (i.e. 4 FWHM from the peak centre position). The standardised multichannel variances for $t_{max}=8\sigma$, i.e. $_{R<1}{}^{m}V_{8}$, are only about 30% higher than the inherent variances $_{R<1}{}^{m}V_{\infty}$ requiring an infinite background region; doubling the background region to $t_{max}=16\sigma$ results in only 15% reduction in variance.

It should be pointed out that these theoretical improvements in $^{m}V^{B}$ with larger background regions rest on the assumption that all parts of the background region are perfectly correlated. In real spectra, however, the further a particular background region lies away from a peak, usually the poorer will be its correlation with the

background directly under the peak. This diminishing correlation in real spectra soon balances out the small improvements in variance that theoretically could be gained by greatly increasing the total background region.

On the other hand, when the available background region is reduced below $t_{max} \sim 4\sigma$ the variances deteriorate very rapidly. When this happens on one side of a peak then the other side should be more heavily relied upon for the combined two sided evaluation of the peak. Evaluations for $t_{max} < 2\sigma$ are made usually when there are overlapping or unresolved peaks that are uncorrelated. This case need not be treated here.

Comparison of the various single-channel schemes, Figures 6.6a to 6.8a show that the variances $^{3:2}v$ of the pseudo-two-channel scheme in very restricted background regions ($t_{max} < 2\sigma$) tend to those of the three channel scheme and at very wide background regions approach the variances ^{2}v of the two-channel scheme.

It may be seen that, as is to be expected, the variances decrease as more discriminators and counting channels are added. The biggest decrease occurs at the first addition and further additions give rapidly diminishing returns. The total possible decrease is not very large. For $R <= 1$ and $t_{max} => 4\sigma$ the variance even in the two-channel scheme is never more than 18% higher than that in the multichannel scheme; the same holds for large ratios $R > 1$ and $t_{max} => 5\sigma$. In single-peak evaluation the simplicity of calculation in two counting-channel schemes leaves little incentive, as far as variance improvement is concerned, for using schemes with

more than two counting channels.

The most widely used scheme is the pseudo-two-channel scheme. Even in the majority of multichannel measurements the peaks are still evaluated according to the pseudo-two-channel scheme. The only basic difference between the little-used two-channel and the pseudo-two-channel schemes is that at a substantial saving of two discriminators the two channel scheme has a slightly higher variance, as shown in Figure 6.6a and 6.7a, particularly at low values of t_{max}. The wide acceptance of the pseudo-two-channel scheme cannot be ascribed to the above difference. It probably stems from the misconception that the pseudo two channel scheme is much more precise or it may have been adopted to simplify calculation. Certainly there is a general unawareness that a two-channel scheme can be implemented by placing both a wide and a narrow single-channel analyser window symmetrically over a peak, the wider counting channel including the narrower counting channel. The algorithms for this overlapping two channel scheme are still just as simple -

$$\begin{vmatrix} P \\ B \end{vmatrix} = \frac{1}{D} \begin{vmatrix} t_1+t_2 & -t_1 \\ -G_1-G_2 & G_1 \end{vmatrix} \begin{vmatrix} Y_1 \\ Y_1+Y_2 \end{vmatrix}$$

where $D = G_1 t_2 - G_2 t_1$

$$\frac{P}{B} = \frac{(t_1+t_2)Y_1/(Y_1+Y_2) - t_1}{-(G_1+G_2)Y_1/(Y_1+Y_2) + G_1}$$

In the pseudo-two-channel scheme the outer counting channel pair is normally placed by inspection far enough for the assumption that $G_2=0$; in the two-channel scheme a similar, somewhat better, approximation $G_1+G_2=0,5$ (per side)

can be made for large enough t_{max}.

In conclusion it can be stated that with an appropriate setting of two pairs of discriminators, the simple two-channel scheme leaves little room for improvement in single-peak evaluation. The far more widely used pseudo-two channel scheme at a 50% increase in the number of discriminators can yield variances in R only marginally better.

7 EVALUATION OF SPECTRA FOR GOLD ANALYSIS

In this chapter the foregoing theoretical results for a single Gaussian peak on a uniform background are applied to the measured spectrum. In gold ore analysis, the relevant part of the spectrum for detailed evaluation consists of a number of gold K X-ray peaks and interfering peaks on a sloping background.

The basis for comparison of spectra is introduced below. Thereafter the spectra from Ba-133, Cd-109, Gd-153, Co-57 and Te-123m excitation are semiquantitatively compared and finally the Cd-109 spectrum will be treated qualitatively in more detail.

7.1 Comparison of different peaks and backgrounds

In the previous chapter, variances were obtained which permitted the comparison of evaluation methods for a single peak on a normalized background. For comparison of the precision or detection limits of different peaks on their particular backgrounds, either the coefficient of variation of the ratios, $CV[R] = \sqrt{V[R]}/R$ i.e. the relative standard deviation at equivalent background counts, or the relative measurement times at a constant background rate to obtain a constant $CV[R]$ may be used. This is basically the same approach as in the previous chapter, although previously standardised conditions allowed some simplification.

At low peak-to-background ratios, i.e. $R<1$, $V[R]$ was

shown to be nearly independent of R because it is dominated by the background so that CV[R] is inversely proportional to R i.e.

$$CV[R] \cong 1/R \qquad \text{(for small R)} \qquad 7.1$$

Because the variance of the mean of a number of independent measurements is equal to the variance of the individual measurements divided by the number of measurements, the coefficient-of-variation of a given R is inversely proportional to the square root of the background count B, or the square root of the measurement time at a constant background rate T_B i.e.

$$CV[R] \propto 1/\sqrt{B} \qquad \text{(R constant)} \qquad 7.2a$$

$$\text{or } CV[R] \propto 1/\sqrt{T_B} \qquad \text{(R constant)} \qquad 7.2b$$

It follows that, for different ratios, the same CV will be obtained with background counts B, or measurement times at a constant background rate T_B, that are inversely proportional to the square of the ratio i.e.

$$B \text{ and } T_B \propto 1/R^2 \qquad \text{(CV constant; R small).} \qquad 7.3$$

Similarly the same CV will be obtained with peak counts P, or measurement times at a constant peak rate T_P, that are inversely proportional to (the first order of) the ratio i.e.

$$P \text{ and } T_P \propto 1/R \qquad \text{(CV constant; R small)} \qquad 7.4$$

These relationships emphasise that the more prominent peaks generally have a lower CV[R]. The ratio has a stronger influence on the coefficient-of-variation than the actual counts. When there are two or more intensity-correlated peaks in a spectrum, it is usual to analyse only the most prominent peak in single-element analysis. When highly efficient spectral evaluation is desired, it may be

worthwhile to look also at the less prominent correlated peaks in order to reduce the total coefficient-of-variation.

7.2 Comparison of spectra from different sources

Sources of five radioisotopes, Ba-133, Cd-109, Gd-153, Co-57 and Te-123m, were used for XRF excitation of the same gold ore sample. The relevant spectra are shown in Figure 7.1. Ba-133, Cd-109, Co-57 and Te-123m showed prominent gold Kα or Kβ' peaks. With Gd-153 the background in the peak regions was much higher and the peaks were no longer discernible above the background noise.

If sources of sufficient strength are available, then the measuring instrument can be operated at its optimum count-rate-handling capability, irrespective of the type of source used. An objective comparison of measurement times required to achieve the same precision when using different types of sources can then be made by normalizing the spectra to the same total count. The count rate handling capability of a measuring instrument, however, depends to some extent on the average energy of the photon flux. Cobalt-57 and Te-123m spectra have average photon energies about 30% and 50% higher than a comparable Cd-109 spectrum. The comparisons below referring to spectra of the same total count, will thus be biased conservatively against Cd-109.

The source excitation efficiency shown in chapter 3 (Table 3.1), when multiplied by the relative intensity of the gold K line from Table 7.1, gives a rough indication of the relative peak height to be expected in a normalized spectrum. Additional source lines, matrix enhancement, and different absorption of Kα and Kβ lines, modify the relative peak height somewhat.

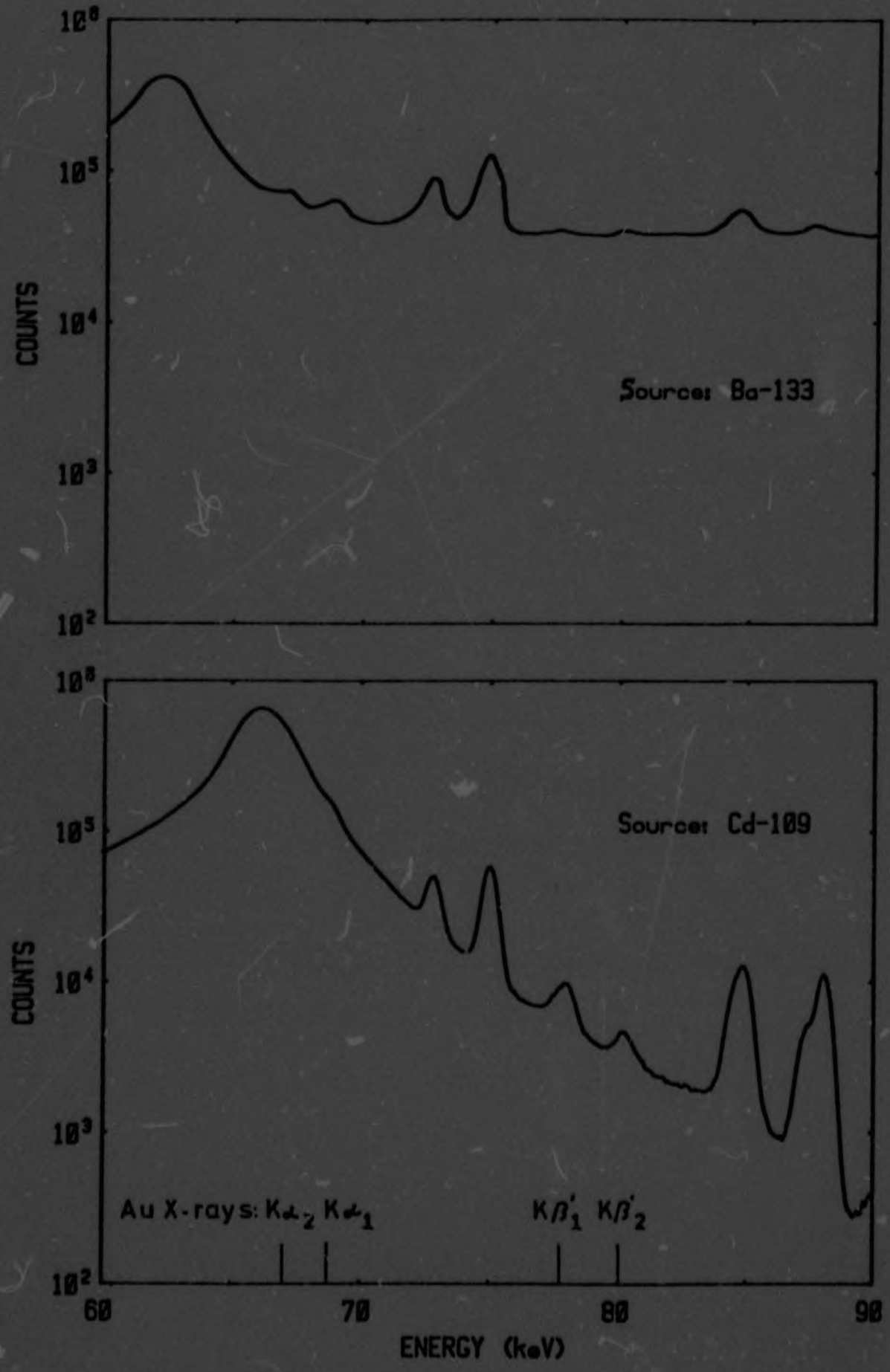


Fig. 7.1 Fluorescence spectra of a standard gold ore sample

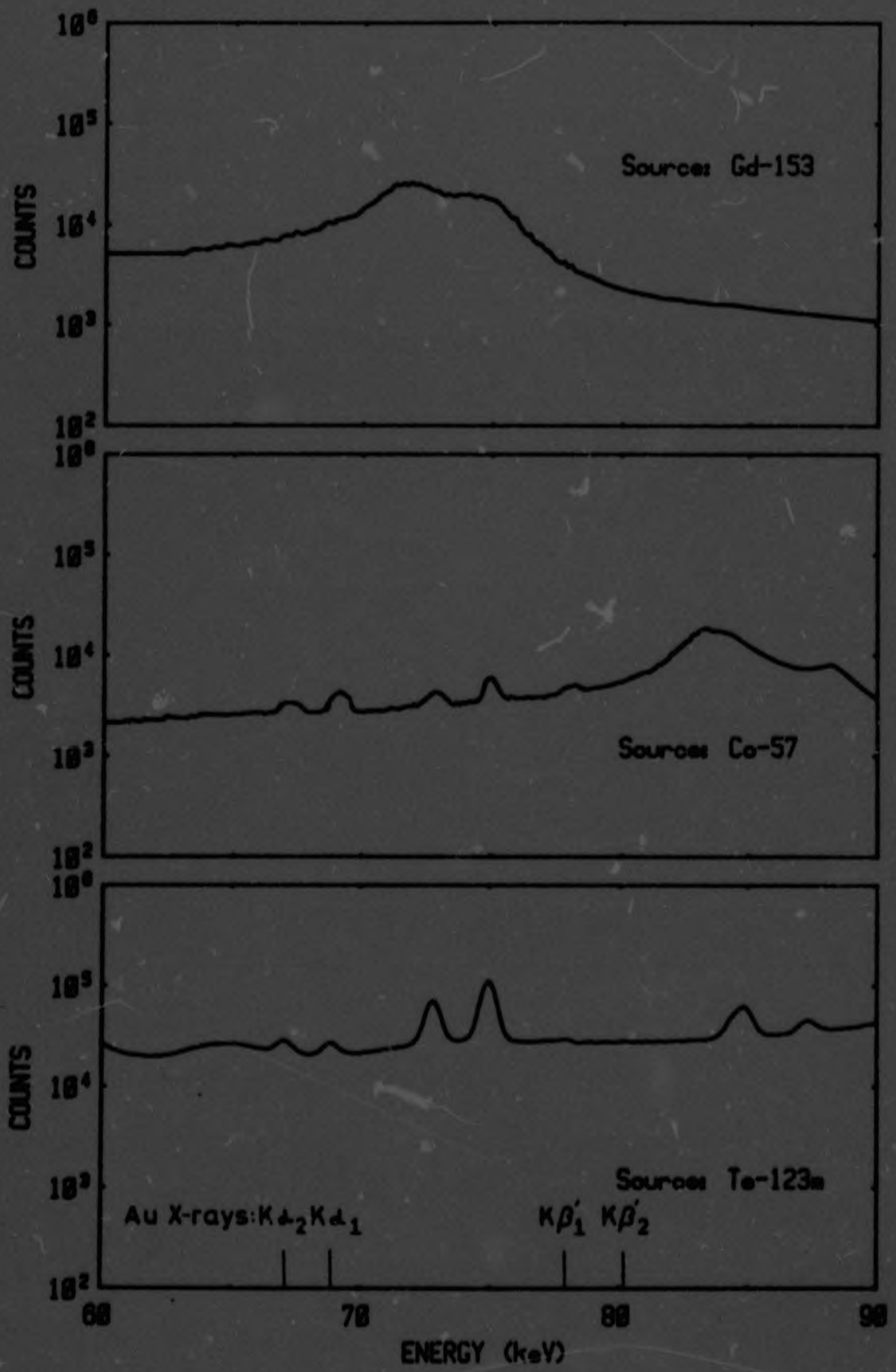


Fig. 7.1 (continued)

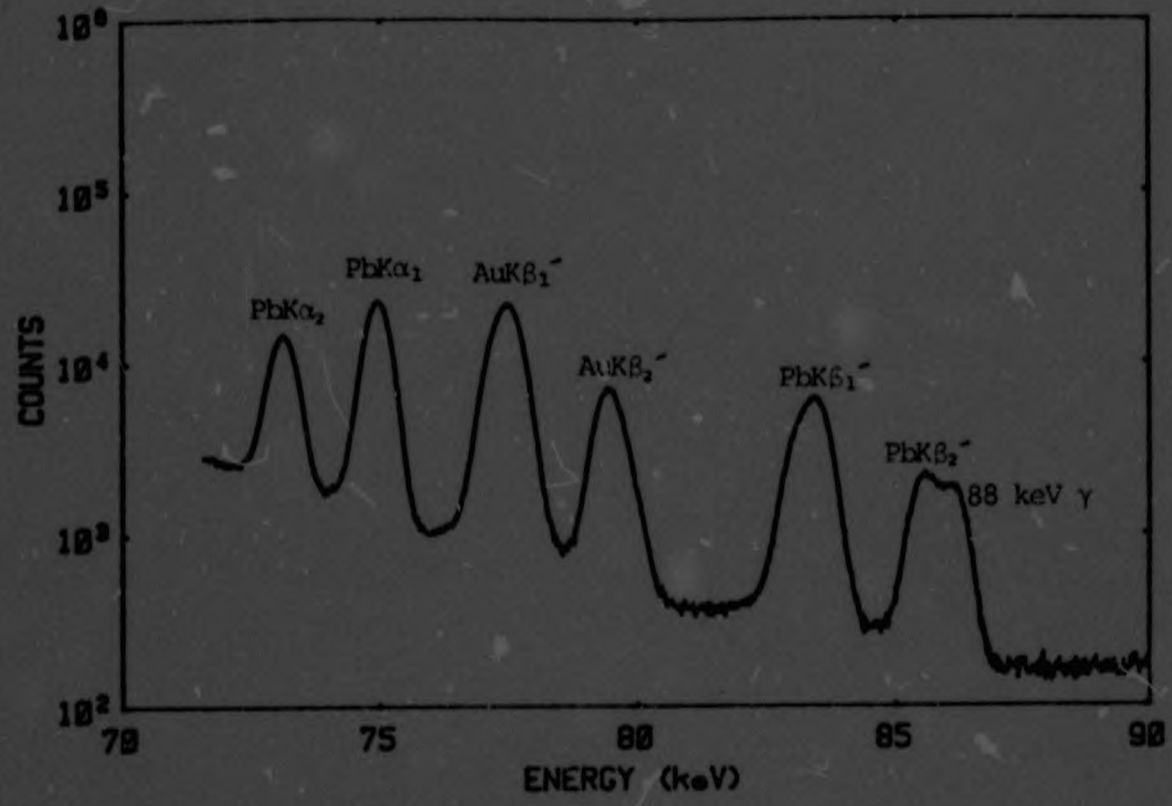


Fig. 7.2 Fluorescence spectra of pure gold and lead

Table 7.1 Energy and relative intensity of the K X-rays of gold and lead

Element	$K\alpha_2$	$K\alpha_1$	$K\beta_1'$	$K\beta_2'$
Gold	66,99(55*)	68,8 (100)	77,9(35)	80,1(9)
Lead	72,80(55)	74,97(100)	84,8(35)	87,3(10)

* Measured relative intensities from 'infinite' sample differ a few percent from the listed values because of matrix absorption.

Author Rolle R
Name of thesis Gamma Ray Fluorescence for In Situ evaluation of ore in Witwatersrand Gold Mines 1979

PUBLISHER:
University of the Witwatersrand, Johannesburg
©2013

LEGAL NOTICES:

Copyright Notice: All materials on the University of the Witwatersrand, Johannesburg Library website are protected by South African copyright law and may not be distributed, transmitted, displayed, or otherwise published in any format, without the prior written permission of the copyright owner.

Disclaimer and Terms of Use: Provided that you maintain all copyright and other notices contained therein, you may download material (one machine readable copy and one print copy per page) for your personal and/or educational non-commercial use only.

The University of the Witwatersrand, Johannesburg, is not responsible for any errors or omissions and excludes any and all liability for any errors in or omissions from the information on the Library website.